

Using multi-platform remote sensing methods to map chenopod shrubland communities in Witchelina Nature Reserve in SA Arid Lands

By

Yun Guang Jasper Wong

Thesis

Submitted to Flinders University for the degree of

Masters of Geospatial Information Science

College of Science and Engineering

22 October 2021

SUMMARY

Environmental monitoring over a large expanse in remote areas is difficult with traditional in-situ vegetation surveys. Remote sensing (RS) helps to overcome the problem by balancing the need to monitor a large study area with adequate spatial resolution to detect the object of interest across a large area. This study uses high-resolution 0.5 metre Pleiades satellite imagery, together with imagery from aerial surveys at 0.03m spatial resolution taken with a camera mounted on an Unmanned Aerial Vehicle (UAV) which acts as pseudo ground control. Classification of the Pleiades imagery is being used to map chenopod shrubs with 2 distinct spatial distribution patterns in Witchelina Nature Reserve (WNR) located in the western Flinders Ranges in the South Australian Arid Lands, a region that covers more than half of South Australia, bordering with New South Wales, Northern Territory and Queensland.

The objective of this study was to employ machine learning methods to achieve high-resolution and accurate mapping of the chenopod habitat of the endangered Thick-billed Grass Wren (TBGW) from a high-resolution satellite imagery. A detailed comparison was made between four vastly different methods of image classification: a) Unsupervised ISO Pixel-based classification; b) Supervised Maximum Likelihood (ML) Pixel-based classification; c) Object-based Image Classification using segmentation- Support Vector Machines (SVM) and d) Object Classification using Deep Learning (DL)- Convolutional Neural Network (CNN).

Accuracy was assessed using withheld pseudo ground truth data and suitability for objective. Results obtained showed that classification accuracy for object-based methods are sufficiently accurate and that RS methods can be used to map the whole of WNR with cost-effective means to support the planning of conservation activities.

DECLARATION

I certify that this thesis does not incorporate without acknowledgment any material previously submitted for a degree or diploma in any university; and that to the best of my knowledge and belief it does not contain any material previously published or written by another person except where due reference is made in the text.

Signed Jasper Wong

Date 22/10/2021

ACKNOWLEDGEMENT

I would like to thank my supervisor, David Bruce, whose guidance, and advice rendered during my time in Flinders University had helped me tremendously for a student with no prior background in this fascinating world of remote sensing.

I would also like to thank the Geospatial Sciences Department who rendered their assistance during technical difficulties with equipment and logistics.

Thanks also go to staff and rotational land managers of Witchelina and Nature Foundation, who assisted me for my first trip to outback South Australia and provided me with the help I needed while organising my trip to WNR and provided me with information and first-hand knowledge of the area.

Lastly, I would like to thank my partner, who has supported me throughout my time in the GIS program.

Contents

SUMMARY	ii
DECLARATION	iii
ACKNOWLEDGEMENT	iv
ACRONYMS & ABBREVIATIONS	vii
LIST OF TABLES.....	viii
LIST OF FIGURES	ix
1. INTRODUCTION	1
2. STUDY AREA.....	6
3. LITERATURE REVIEW.....	8
3.1 Vegetation Mapping using Remote Sensing in Australia.....	8
3.2 Satellite Remote Sensing -collecting data from the environment.....	10
3.2.1 A plethora of information- spectral, spatial, and radiometric details	12
3.2.2 Satellite remote sensing in the arid lands.....	14
3.2.3 Using other remote sensing dataset to augment Satellite Imagery	19
3.3 Image Classification Approaches.....	20
4. METHODOLOGY.....	30
4.1 Mapping vegetation and Classification Schema.....	30
4.2 Methodology Flow Chart.....	36
4.3 Data Acquisition.....	36
4.3.1 Obtaining Pleiades Imagery of study area	36
4.3.2 Pre-calibration of Pleiades Imagery.....	37
4.3.3 18 UAV surveys over study area from 5 th -7 th August 2021	39
4.3.4 Processing Ortho-imagery in Pix4D.....	41
4.4 Image Classification Tools	45
4.4.1 Unsupervised ISO Pixel-based image classification	47
4.4.2 Supervised Pixel-based image classification- Maximum Likelihood.....	47
4.4.3 Object-based Image Classification using Support Vector Machine (SVM).....	47
4.4.4 Object Classification using Deep Learning- Convolutional Neural Network (CNN)	49
4.4.5 Measuring Accuracy of the results from the four methods	54
5. RESULTS	58
5.1 Unsupervised Pixel-based Image Classification Results	59
5.1.1 Accuracy Results	60
5.2 Supervised Pixel Classification Results.....	61
5.2.1 Accuracy Results	62
5.3 Segmentation Results.....	63

5.3.1 Accuracy Results	63
5.4 Object Classification using Deep Learning.....	65
5.4.1 Attempt 1- Classification Results using image_chip size 128 x 128.....	65
5.4.2 Attempt 2- Classification Results using image_chip size 64 x 64.....	68
5.5 Summary of Accuracy Metrics for the four methods for Chenopod Classes.....	71
5.6 Visual Comparison of Results for two selected areas- Area 2a, 1f.....	73
6. DISCUSSION.....	75
6.1 Overall Results	75
6.2 Limitations of Pixel-based Classification	76
6.3 Limitations of Object-based segmentation classification	78
6.4 Limitations of Deep Learning- CNN	78
6.5 Comparison of classification methods.....	80
6.6 Potential datasets to augment image-based classification	81
7. CONCLUSION	83
8. REFERENCES	85
9. APPENDICES.....	91
9.1 Appendix A- Map of Study Area and Witchelina Station Map.....	92
9.2 Appendix B- Metadata of Pleiades Imagery	94
9.3 Appendix C- Ground Control Points for UAV Survey Missions.....	100
9.3 Appendix D- Field Notes taken using Survey 123.....	101
9.4 Appendix E- Maps of Classification Results.....	101
9.4.1- Unsupervised ISO Pixel Classification	102
9.4.2- Supervised ML Pixel Classification.....	103
9.4.3- Object-based Image Segmentation- SVM.....	104
9.4.4- Object-based Image Classification using Deep Learning	105

ACRONYMS & ABBREVIATIONS

GPU Graphics Processing Units

GSD Ground Sampling Distance

HR High Resolution

LULC Land Use Land Cover

ML Maximum Likelihood

MS Multispectral

MVG Major Vegetation Group

NF Nature Foundation

NVIS National Vegetation Information System

PS Pan-sharpened

RGB Red-Green-Blue

RS Remote sensing

SVM Support Vector Machine

TBGW Thick-bill Grass Wren

TERN Terrestrial Ecosystem Research Network

TIFF Tagged Image File Format

WNR Witchelina Nature Reserve

LIST OF TABLES

Table 1- Original Classification schema	31
Table 2- Final classification schema- chenopod classes	33
Table 3- Definition of chenopod classes by density of chenopod shrubs	34
Table 4- Final Classification Schema- Non-chenopod classes	35
Table 5- Processing level of Pleiades imagery ordered from Airbus.....	37
Table 6- Pixel Values (Digital Numbers) Statistics of Pleiades Imagery	37
Table 7- Details of each survey area.....	40
Table 8- Samples for Supervised Pixel-Based Image Classification.....	47
Table 9- Samples for Segmentation using SVM.....	48
Table 10- Training Samples used for training the deep learning model.....	51
Table 11- Parameters of Training DL Model.....	51
Table 12- Accuracy Samples for reference dataset.....	55
Table 13- Confusion Matrix for Unsupervised Classification.....	60
Table 14-Confusion Matrix for Supervised Pixel Classification	62
Table 15- Confusion Matrix for Object-based Classification-SVM	63
Table 16-Confusion Matrix of Training Model of DL Attempt 1- The precision scores and recall scores.....	66
Table 17- Confusion Matrix of Training Model of DL Attempt 1- The precision scores and recall scores.....	69
Table 18- Confusion Matrix for Classify Objects using DL (2nd attempt)	Error! Bookmark not defined.
Table 19- Summary of selected accuracy metrics	Error! Bookmark not defined.

LIST OF FIGURES

Figure 1-Map of Study Area	6
Figure 2- study area extent (approximate) 1: 200,000	7
Figure 3- Thematic Map of WNR (Department of Water, Land, and Biodiversity Conservation 2009)	7
Figure 4- Adapted from Systems Analysis for Sustainable Engineering, (Ni-Bin 2011).....	10
Figure 5-Three different considerations when selecting a satellite image for analysis	11
Figure 6- Reflectance characteristics in the visible and reflective infrared range (Richards 2013: 11).....	13
Figure 7- Comparison of spectra of vegetation from humid and arid environment (Okin and Roberts 2004: 12)	16
Figure 8- Extracted from 'UAVs and Machine Learning Revolutionising Invasive Grass and Vegetation Surveys in Remote Arid Lands' (Sandino et al. 2018).....	27
Figure 9- Classification flow-chart	36
Figure 10- Initial Processing in Pix4D.....	42
Figure 11- Point Cloud densification in Pix4D	42
Figure 12- DSM Processing Options in Pix4D. Note GSD is slightly different for each orthomosaic.	43
Figure 13- UAV surveys carried out at study area from 5th -7th August	43
Figure 14- Area 4d	44
Figure 15-Area 2 (a,b,c,d)	44
Figure 16- Area 1 (a,b,c,d)	44
Figure 17-varied background where chenopod shrubs are present.....	45
Figure 18- Object-oriented feature extraction workflow, extracted from (ESRI 2021)	48
Figure 19-Spectral Profile of classes.....	49
Figure 20- Distribution of training samples across study area	50
Figure 21- Sample Training Chips for both attempts	52

Figure 22- Sample Training Chips according to labels (classes)	53
Figure 23-Sample of accuracy reference polygons Scale 1:6613.....	55
Figure 24- Multiclass metrics derived from a confusion matrix, adapted from (Maxwell, Warner & Guillen 2021: 6).....	56
Figure 25- Manual Accuracy Assessment Tool Check for DL Results	57
Figure 26- Sample of random accuracy points	57
Figure 27- 220 Accuracy points distributed across processed DL results	57
Figure 28- Classified Results from Unsupervised ISO Pixel-based Method.....	59
Figure 29-Classified Results from Supervised ML Pixel-based Method.....	61
Figure 30- Classified Results from Object-based Segmentation-SVM.....	63
Figure 31- Classified Results from DL- Attempt 1.....	65
Figure 32-Loss Graph and Confusion Matrix (Attempt 1)	66
Figure 33- Classified Results from DL- Attempt 2.....	68
Figure 34- Loss Graph and Confusion Matrix (Attempt 2)	69
Figure 35- Area 2a- Scale 1:1,1849 In order of results: Orthoimage (ground truth), Unsupervised ISO Pixel Classification, Supervised Pixel Classification, Object-based Classification using SVM, Object-based classification using DL (128*128), Object-based classification using DL (64*64)	73
Figure 36- Area 1F- Scale 1:1,1849 In order of results: Orthoimagery (ground truth), Unsupervised ISO Pixel Classification, Supervised Pixel Classification, Object-based Classification using SVM, Object-based classification using DL (128*128), Object-based classification using DL (64*64)	74

1. INTRODUCTION

Environmental monitoring in arid regions can be achieved through employing various remote sensing (RS) methods in order to meet multiple environmental objectives for the user. This research thesis demonstrates the use of multiplatform RS and image classification methodologies to produce a thematic map, mapping objects of interest for land and conservation managers in order to support their conservation efforts in a private nature reserve, managed and owned by Nature Foundation (NF), a conservation organisation based in Adelaide. Witchelina Nature Reserve (WNR) is a 421,000-hectare former pastoral property that was purchased by Nature Foundation in 2010 for conservation.

Nature Foundation, a conservation organisation founded in 1981, managing several properties across South Australia faces the problem that most landowners have with their property- the large expanse with limited manpower and resources makes it difficult for the Land managers to manage assets and resources across their property.

As a conservation organisation focused on land acquisition for conservation, NF manages a few properties that are vast in size but with limited rotational land managers for conservation activities including removal of weeds, de-fencing and baiting of predators. These interventions often do not have the support of monitoring schemes because of issues of accessibility, vastness, resource constraints.

At WNR, land managers are rotated regularly to help with conservation management activities including de-stocking of cattle, weeds removal, baiting of predators and de-fencing. Given the large expanse of land with limited time and resources, RS can help land managers make decisions on where best to focus conservation activities and assess the effectiveness of their conservation efforts.

Due to WNR's previous existence as pastoral land and its subsequent conversion into conservation land from 2010, it represents a unique proposition as prime conservation land in the middle of the arid region in South Australia and an opportunity to compare biodiversity

levels and ecological status when it was under pastoral ownership and its current incarnation as conservation land to measure the impact of conservation activities undertaken in the area.

Hence, numerous researchers have carried out research studies and experiments in diverse disciplines across ecology, biology among others in the past years (Namyatova, Schwartz, and Cassis 2013; Namyatova, Elias, and Cassis 2011; Woinarski et al. 2017; Slender et al. 2018).

In terms of its biodiversity value, WNR is significant as it forms a strategic habitat link from Lake Torrens in South Australia into the Northern Territory functioning as “the world’s first transcontinental wildlife corridor” between Port Augusta and Arnhem Land (Department of Agriculture Water and the Environment 2021). It serves as a refuge for many animals including the nationally vulnerable Eastern Thick-billed Grass Wren (*Amytornis modestus*) (TBGW), protecting unique ecosystems not found in other parks and reserves.

Following a discussion with the Science and Knowledge Program Manager from Nature Foundation, the following research objectives were identified:

1. Explore detailed mapping of chenopod shrubs and its distribution in Witchelina Nature Reserve
2. Undertake broad-level mapping of the WNR to help inform conservation efforts in the privately-owned nature reserve and also fill a knowledge gap in state-level vegetation mapping

Chenopod shrublands were selected as the main object of interest as prior extensive surveys of these shrublands had not been done before. As the primary habitat of the endangered TBGW, mapping chenopod shrublands will yield insights into the distribution of the habitat of the TBGW and help with the conservation strategies of the endangered wren.

Thick-billed Grass Wren (TBGW) and its habitat link to Witchelina Nature Reserve

Louter (2016) examined the relationship between habitat restoration of the nationally vulnerable thick-billed grass wren, mainly found in arid regions of South Australia and New South Wales, and its influence on the population of the threatened wren with a study from 2012-2015 conducted at Witchelina Nature Reserve, a formal pastoral station. The reserve lies within the range of the TBGW spanning three bioregions, Willouran, Mulgarie, and Marree – see figure 3 for location of Willouran- (Louter et al. 2015: 18).

Located in the Australian arid zone means that the environment is prone to developing heterogenous ecological landscapes with irregular soil types and limited sporadic rainfall, creating patchy distributions of plant communities which greatly affects the animals living in the arid zone (Tongway and Ludwig 1980; Ford 1987; Martin 2006 cited in Slender et al. 2017: 273).

TBGW generally live in saltbush (*Rhagodia* sp.), blue bush (*Maireana* sp.) cotton bush (*Maireana* sp.), rock samphire (*Crithmum* sp.) and grasses on watercourse and among flood debris (Schodde 1982; Serventy 1982; Rowley and Russell 1997 cited in Louter 2016: 7).

Mapping Plant Functional Types (PFT)

Mapping individual shrub and plant communities requires distinct approaches for the segmentation process. The former requires the RS analyst to specify the minimum number of pixel (relating to its size) to consider detecting an individual shrub so non-mature shrubs can be filtered out of the classification. For the latter, the plant community can be described by either the species of flora in the community or by its Phyto physiognomy (its structure) (Ustin and Gamon 2010: 797). For example, a wide open shrubland may comprise of dense covering of shrubs interspersed with short trees like acacias and forbs.

Any remote sensing method needs to acutely define the object of interest to collect relevant data on it. While broad classification makes this task relatively straightforward (e.g., buildings vs non-buildings, vegetation vs non-vegetation), mapping a plant group is a more difficult task

due to the “small inter-class variance between visually similar sub-classes” and the contextually rich sub-categories in the world of taxonomy (Cai et al. 2019: 166).

In ecological science, taxonomy is viewed through the lens of the plant group’s functional type that uses “structural, physiological and/or phenological features” grouping species in response to environmental conditions or impacts on ecosystems (Ustin and Gamon 2010: 796).

Chenopod shrubs, samphire shrublands and forblands- Major Vegetation Group 22

The habitat of the TBGW all generally fall under the Chenopodiaceae family vegetation major group and appear most commonly with acacia covering more than a quarter of the Australian continent as open shrubland, lying entirely within the arid zone on “extensive clay plains, gibber hills and plains, aeolian sandplains and hypersaline flats” (Foulkes et al. 2014: 439); (Commonwealth of Australia 2017). These plants are slow growing, even without grazing (Slender et al. 2017: 276). They tend to dominate where there is rainfall, with regeneration only possible with prolonged rainfall events, but are both drought and salt-tolerant (Foulkes et al. 2014: 440)

Mapping Habitats

Louter’s vegetation survey in Witchelina Reserve looked at long-live perennial (its cover, abundance, and diversity), limiting it to only adult shrubs larger than 10cm in height, and species belonging to genus, *Rhagodia*, *Atriplex*, *Maireana*, *Eremophila* and *Acacia* (Louter 2016: 21) .

Chenopod vegetation cover was used in analysis for TBGW presence and Louter noted that TBGW were more likely to occur at sites with more chenopod vegetation cover as it signifies shrub abundance and diversity which supports more birdlife. Group vegetation cover maps are too broad for conservation purposes- TBGW do not thrive in any areas with high vegetation cover; while species-level mapping based solely on spectral information of chenopod vegetation cover does not tell us if the chenopod shrubs are mature and wide enough to support the TBGW (Louter 2016: 31).

Nagendra et al. (2013: 48) noted that often, land cover mapping does not translate accurately into habitat mapping as attributing spectral signatures from land cover to finer details in habitat classification is complicated, with the added complexity of a heterogeneous landscape (arid land environments are notorious for that) and requirements of high geometric accuracy.

Some methods were devised to overcome these challenges including the use of fuzzy classification, probability theory and object-oriented method (which this study uses) but ultimately, the choice of remote sensing dataset determines the amount of information to map the complex, fine scale and structurally and floristically variable habitat to sufficient degrees of accuracy. Vegetation surveys previously undertaken by Louter (2016), while useful in establishing a correlation between two variables, is inadequate for mapping the habitat of the threatened TBGW over the entire nature reserve. RS, and this study, thus can play a role in filling that gap in order to support conservation efforts in the nature reserve.

2. STUDY AREA

The study area is bounded by the extent 6674000 N 6664995 S, 209300 E 217000 W (UTM Zone 54S) with an area of 69.34km² or 6934 hectares. It is 1.6% of the entire WNR.

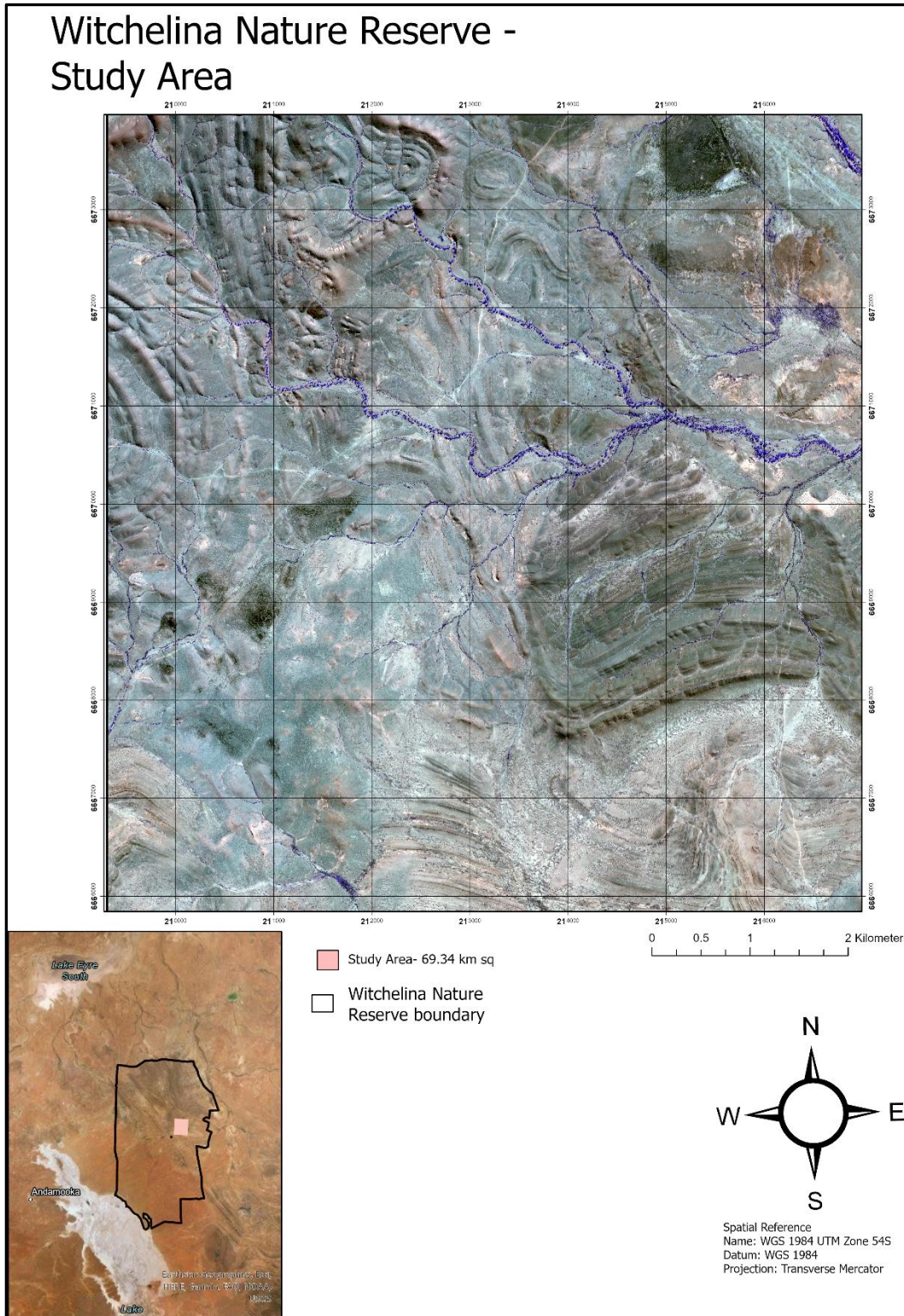
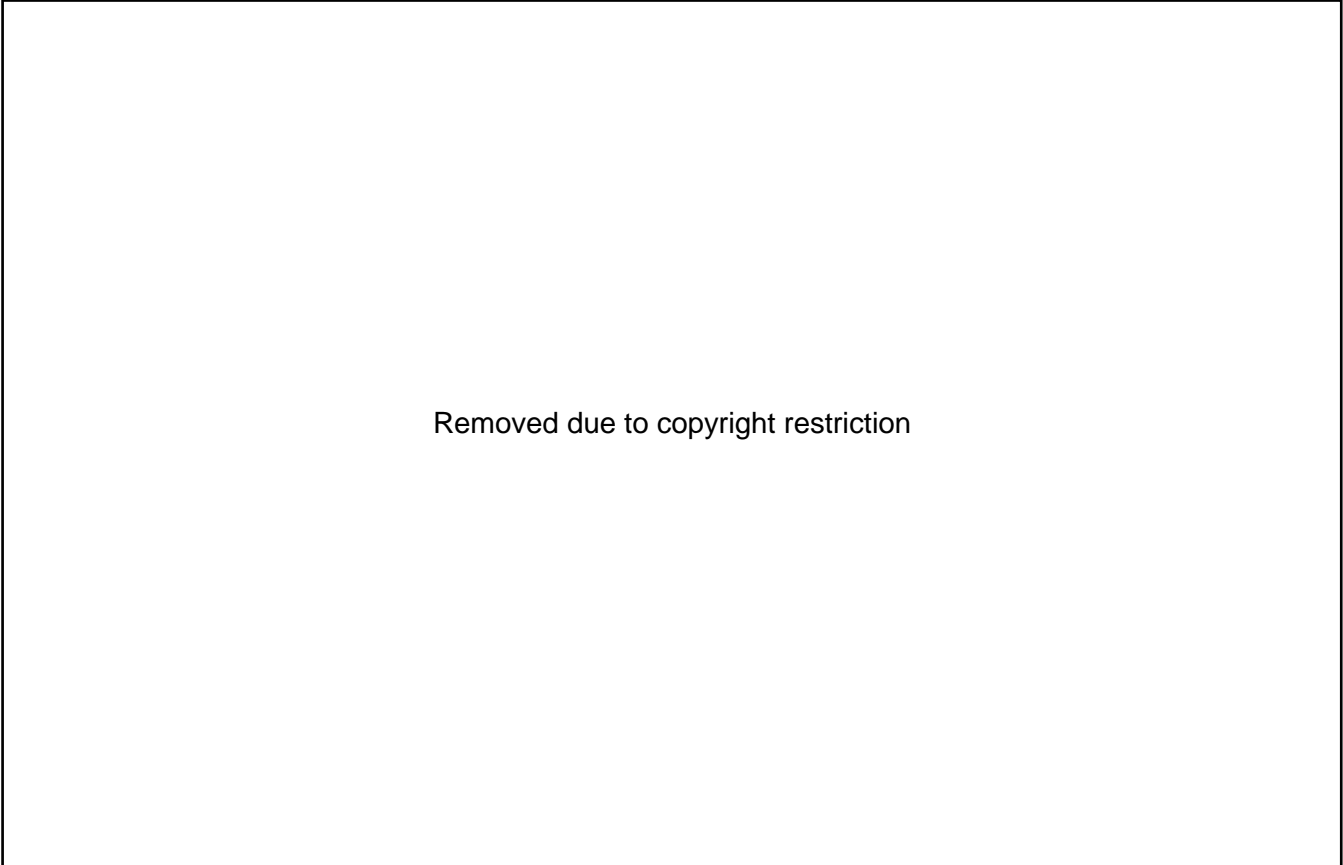


Figure 1-Map of Study Area



Removed due to copyright restriction

Figure 3- Thematic Map of WNR (Department of Water, Land, and Biodiversity Conservation 2009)

The study area is comprised of three distinct bioregions characterised by then Department of Water, Land, and Biodiversity Conservation, which at present is the Department for Environment and Water. The three distinct bioregions are Willouran, Paradise, and Myrtle Louter (2016: 18). TBGW can be found across the entire study area but are especially concentrated in Willouran and Paradise where chenopod shrubs such as saltbush, bluebush, blackbush, and samphires can be found.

3. LITERATURE REVIEW

3.1 Vegetation Mapping using Remote Sensing in Australia

Environmental monitoring is an important process both on its own merit and also as part of the Environment Impact Assessment process for development projects undertaken in Australia and other parts of the world to assess environmental risks and impacts that arise from development projects (Nagendra 2013 :47).

Environmental monitoring is also important for the ecologically sustainable management of natural resources and aids in supporting ecology, environmental management and policy making. (Lindenmayer et al. 2014: 44). These authors for instance recommended long-term ecological studies spanning continuous periods of years which will then allow us to quantify ecological responses to environmental change. Long-term surveys have been instrumental in quantifying effectiveness of conservation management activities which can be linked to the proliferation of individual species that thrive with certain conditions.

Vegetation mapping efforts across Australia

One key example of a monitoring scheme is vegetation mapping which can occur at various levels and scales, including at national, state, or council level. For example, on a national level, the National Vegetation Information System (NVIS) was developed to assess the state of native vegetation in Australia on a timely basis (Department of Agriculture Water and the Environment. 2021). It is also used as input data for other applications, including for carbon accounting, native vegetation and biodiversity reporting, for research and fire modelling (NVIS Technical Working Group 2017: 7). The NVIS manual (version 7.0) sets out a few standards including standards for data management and compilation, taxonomic attributes, vegetation condition attributes, standards for vegetation spatial data, among others.

Vegetation mapping efforts exist nationally under the guide of the federal Department of Agriculture, Water and the Environment on the NVIS which “provides information on the extent

and distribution of vegetation types in Australian landscapes.” (Department of Agriculture Water and the Environment 2020). It is managed through the NVIS technical Working group established in 2015 which publishes the Vegetation Attribute manual for the ongoing development of the NVIS.

Under the NVIS, there are 32 classified major Vegetation groups based on an aggregation of NVIS level five-six types based on dominant genus-plus categories. Example groups are: MVG 1- Rainforest and vine thickets; MVG 3- Eucalypts open forests. MVG 13- Acacia open woodlands and MVG 22- Chenopod shrublands, samphire shrublands and Forblands (NVIS Technical Working Group 2017).

In WNR, MVG13 and MVG 22 are the two most dominant groups with the latter the focus of the study area in this study.

Other state-specific vegetation mapping guidelines also exist. One such guideline is the Native Vegetation Council rangelands assessment manual developed to assess native vegetation systems in the arid zone of South Australia (managed under the SA Arid Lands board and Alinytjara Wilurara (AW) board) for purposes like including clearance or regulation application areas, demarcating potential and established Significant Environmental Benefit offset areas, and Heritage agreements (Natural Resource South Australia 2017).

On the academic front, terrestrial ecosystem research network (TERN) involving various universities across the country, provides spatial data products at regional and continental scales to characterise and monitor Australian ecosystems over time. The data on the platform include land cover data, vegetation composition, fire dynamics, field survey datasets, attributes of soil, and landscape attributes including slope, aspect, solar radiation, etc. (TERN 2021). These research-focused projects fill in the need for more comprehensive monitoring projects carried out in smaller, critical areas which helps to support state-level and national vegetation mapping efforts at a coarser scale.

TERN is also dedicated to using remote sensing techniques to characterise and monitor Australian landscapes. It uses a mix of space-borne, airborne and in-situ remote sensing equipment for its diverse product offerings. At present, it is developing case studies for UAV multispectral data collection for producing fractional cover and canopy structure products, satellite imagery correction from the *Himawari* satellite, and blending multi-sensor reflectance. (TERN 2021).

3.2 Satellite Remote Sensing -collecting data from the environment

Remote sensing, which is one of the two primary ways to collect data in the environment, the other being in situ monitoring, contributes to information gathering, that becomes knowledge with context provided by the domain expert that can be translated into action by the land manager or government department responsible for the area (See Figure 4 below)



Figure 4- Adapted from *Systems Analysis for Sustainable Engineering*, (Ni-Bin 2011)

As a remote sensing method, satellite-based imagery is one of the most popular platforms due to its relatively ease of accessibility and multiple applications. There exists a multitude of methodologies using active or passive sensors, and through spaceborne (land observation satellites), airborne (UAVs or planes) or in-situ sensing equipment (ground spectroradiometers using field methods like transects). Under passive sensors on earth observation satellites, there are panchromatic, multispectral, and hyperspectral sensors. With active sensors, we have synthetic aperture radar (SAR) and Light Detection and Ranging (LiDAR)

The choice of sensors depends on the variable to be observed, keeping in mind that the choice of satellite imagery is also a compromise of the issues presented in figure 5:

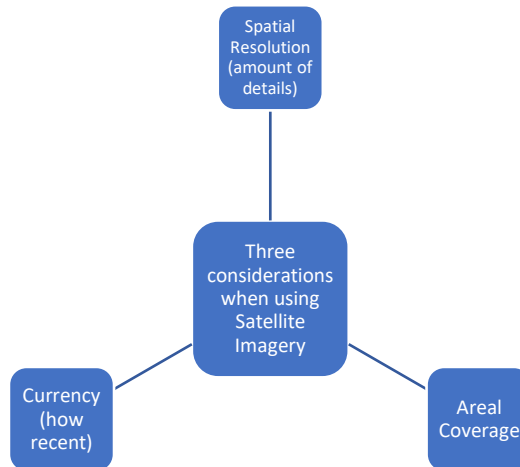


Figure 5-Three different considerations when selecting a satellite image for analysis

The ideal satellite image would cover the entire study area (wide areal coverage), have high spatial, radiometric, and spectral resolution (sub-meter spatial resolution, 12-bit radiometric resolution-, many more than 4 narrow spectral bands), and high temporal resolution (daily coverage). This ideal satellite imagery does not exist unfortunately, and even if it did, would be very costly to obtain. Compromises are often made when considering the objectives of the research and characteristics of the study area.

Because of its wide areal coverage, satellite imagery has played an important role as a remote sensing method for land cover monitoring and thematic mapping.

The first wave of studies employing remote sensing of vegetation was first driven by “environmental monitoring” satellites like the Landsat Thematic Mapper with 30m MS resolution and 15m Pan resolution, which allows monitoring “physiognomy, cover type and fractional canopy cover.” (Ustin and Gamon 2010: 799), the second group of satellites monitored vegetation structure and phenology to monitor climate response (Tucket et al. 1985 cited in Ustin and Gamon 2010: 799) while the third group of satellite allowed access to sub-meter resolution civilian satellites which allowed accurate measurement of vegetation by species-level augmenting vegetation field surveys.

The wide array of remote sensing sensors means that there is a wide choice of satellite imagery for analysis, and each would need adjusted approaches towards processing them in order to retrieve the desired information. RS is vital for the monitoring of environmental resources distributed all around the world and conservation monitoring which runs the gamut of assessing protected areas, habitat extent and condition, species diversity, and threats. (Andrefouet et al. 2003; Goetz et al. 2003; Sawaya 2003; Kayitakire et al. 2006; Wang et al. 2004 cited in Poon 2007: 76; Nagendra et al. 2013). The wide range of applications and objectives mean that a universal criterion for choosing a feasible sensing technology and data processing steps has not yet been, and may not be defined (Sandino et al. 2018: 2)

In addition to space-borne satellite imagery, the availability of alternatives of other RS data sources (including aerial imagery or aerial LiDAR) means that the former can be augmented with observations from other RS platforms. Aerial imagery captured from UAVs has grown in popularity in recent years due to its accessibility and spatial resolution and is one of the most popular data sources for multi-platform RS for overcoming limitations arising from the sole use of a single platform remote sensing. Examples of these successful studies will be presented in section 3.2.3.

3.2.1 A plethora of information- spectral, spatial, and radiometric details

When a satellite image over a study area is obtained, it comes with a plethora of information: the spectral bands, the spatial resolution of the image, the temporal resolution, and the radiometric resolution which allows the RS user to interpret the values in each band; the object shape and edge; and brightness value from its respective resolution (Richards 2013: 4). This information can be interpreted meaningfully with context to form knowledge about the scene captured in the satellite image. In the natural environment, vegetation, soil, and water, the three major components have different spectral characteristics that allow the RS user to differentiate them based on spectral resolution alone (figure 6). The four typical multispectral bands used in many remote sensing sensors are blue (0.45-0.510 μm); green (0.510-0.580 μm); red (0.630-0.690 μm) and near infrared (0.770-0.895 μm) (Xue and Su 2017: 1).

Spectral Resolution

What most studies have used at minimum is the use of spectral resolution to quantify and map vegetation in their respective study areas. The utility of satellite imagery can be defined by its ability to record “fine details in a distinguishable manner” through its spectral, spatial, and radiometric resolution (Campbell 2011: 285). Spectral resolution works on the premise that physical objects reflect sunlight in different ways due to its chemical composition. The spectral properties of vegetation, in all its diversity, form and species, has a spectral response that is correlated with the biochemical characteristics of the plant (Campbell 2011: 471). For a main component of photosynthetic plants, the higher the amount of chlorophyll, the higher the absorption of red energy and the higher the reflectance of near-infrared energy which can be seen clearly in the spectral graph- see spike in NIR (0.770-0.895 μm) in figure 6 below.



Figure 6- Reflectance characteristics in the visible and reflective infrared range (Richards 2013: 11).

Vegetation indices are common formulae used in remote sensing, to calculate vegetation cover, vigour, or growth dynamics among other applications (Xue and Su 2017: 1). They are calculated by the ratio of reflectance in the red and NIR section to calculate vegetation cover

(Glenn et al. 2008). Normalised Difference Vegetation index (NDVI) is the simplest and most popular index which depends mainly on the reflectance of red and NIR and is strongly correlated with the chlorophyll content- including green biomass and leaf water content (Tucker 1979 cited in Glenn, 2008: 2138). In Xu & Su's review of vegetation indices, they noted over 100 vegetation indices that focus on different spectral bands because of different vegetation properties under different circumstances that can not only improve the detection of green vegetation through adjustment of the reflectance from background soil, but also detect water stress or detect the amount of chlorophyll in the plant (Xue and Su 2017: 7).

Spatial Resolution

The next important resolution would be the spatial resolution of the imagery that allows us to see the shape and form of the image object. The general rule of thumb is a minimum of 3 pixels in order to differentiate objects from other objects (Poon 2007: 45). With the advent of meter and sub-meter resolution satellite imagery, Poon argues that we can move beyond the traditional thematic mapping associated with Land Use Land Cover (LULC) and delve into "exploiting spatial and contextual attributes" with an eye towards metric applications (2007: 27).

Radiometric Resolution

Another less important but relevant resolution is the radiometric resolution of the image. It describes the sensor's ability to discriminate small differences in radiation within a pixel (Poon 2007: 44) which allows the RS user to discern in detail two objects with similar but slightly different spectral reflectance due to its material composition for example. This can be advantageous when trying to quantify nuanced differences in material changes of the object

3.2.2 Satellite remote sensing in the arid lands

In the South Australian outback (also known as the SA Arid Lands in terms of regional land management), its arid environment contains some of the driest part in South Australia and the "largest percentage of intact ecosystems and natural biodiversity" (Department of Environment

and Natural Resources 2020). Given its vastness and relative inaccessibility, it proves a problem for land managers to efficiently deploy resources to help protect wildlife habitat and promote biodiversity over the arid expanse. Conservation efforts are often hampered by lack of knowledge, capacity constraints and lack of resources, key constraints faced among land managers managing large properties (Okin and Roberts 2004; del Río-Mena et al. 2020). One way to overcome the vastness and remoteness of the outback is to use satellite imagery to monitor the vast landscape as it is a time- and cost- efficient method for monitoring change in the desert environment (Okin and Roberts 2004: 1).

As mentioned before, the arid environment is a complex environment that brings with it its own unique challenges for satellite remote sensing. One prominent challenge is the dominance of background effects -due to soil being the dominant land surface in arid environment. Good for geological remote sensing with the absence of vegetation but not great for vegetation remote sensing with vegetation's smaller contribution to the area-averaged reflectance in a pixel (Okin and Roberts 2004: 11).

Some authors have noted the over-estimation of vegetation cover in in darker and bright soils while others have noted that the spectral reflectance for Band 2/4 for the Landsat Enhanced Thematic Mapper Plus (ETM+) does not increase by more than 5% even as the percent of vegetation cover increases from 0% to 100% (Okin and Roberts 2004: 12; Huete et al. 1985 cited in Jafari 2007: 67).

Vegetation in the arid environment also have different spectral response to their counterparts in a more humid environment. This can be seen in the difference in spectral response of Non-Photosynthetic Vegetation (NPV), the most common vegetation present in an arid environment compared with the spectral response of its Green Vegetation counterpart (GV) which is prevalent in humid environments in the NIR wavelength bandwidth circled in red in figure 7:



Figure 7- Comparison of spectra of vegetation from humid and arid environment (Okin and Roberts 2004: 12)

Plants in the arid environments have different considerations from plants in the humid environment. They need to reduce the absorption of photosynthetically active radiation (PAR) (i.e., sunlight) because it is in abundance in the desert while at the same time limit the loss of water through evapo-transpiration thus the area of leaf size is a lot smaller than plants in the humid environment. The highly reflective spines also help to protect the photosynthetic part of the plant.

Another factor of added complexity is that the reflectance can differ based on the state of the vegetation. Desert plants are dormant during most of the year and can appear senesced which is accompanied by a change in spectral reflectance as it turns duller than a plant that is flowering. Other challenges include:

- Exposed and variable soil surfaces can contribute to within-scene variability (true for Witchelina Study Area where Chenopod Shrubs occur both on sandy clay soil as well as dark shale)

- Open canopies contribute to multiple scattering and nonlinear mixing
- Lack of red edge compared to humid vegetation

(Okin and Roberts 2004: 16).

Despite those unique challenges, plenty of researchers have tried to overcome these challenges by inventing new ways circumvent those issues.

One of the earliest applications of remote sensing methods in the arid region was an attempt to map the distribution of distinct biomass- that of the arid shrub and semiarid grassland- in the southern New Mexico desert in the US using airborne digital video imagery, NDVI and spatial statistics (interpolation methods) that required the use of a satellite imagery with high enough spatial resolution- larger than that of the arid shrub- in order to map the former (Phinn et al. 1996). Another study looked into the degradation of arid zones by observing the conversion of arid grasses into woody shrubs that could be monitored by geostatistical and textural analysis of high-resolution satellite image (Okin and Gillette 2001).

Apart from the use of multispectral satellite imagery, there is a small but growing subset of researchers who have employed the use of hyperspectral RS, whether on airborne, satellite, or in situ platforms. Hyperspectral methods use hyperspectral sensors which are able to magnify the standard spectral bands and magnify it to nanometer resolution, allowing the RS user to use spectroscopy to examine fine spectral differences between different objects and objects with different properties.

Studies using hyperspectral RS have looked at vegetation in complex scenes in areas like western Kalahari, Botswana (Meyer & Okin 2015) ; southern Arid Lands of South Australia (Jafari, 2007); east of Terowie, South Australia (Lewis, Jooste & de Gasparis, 2001); Sonoran desert, USA- Invasive Grass Detection (Olsson, van Leeuwen, and Marsh 2011); south-eastern Arizona, USA (Sankey et al. 2018), APY Lands North Western SA (Marshall, Lewis, and Ostendorf 2014), just to name a few.

Often studies using hyperspectral RS to map vegetation employ spectral mixture analysis (SMA) or multiple endmember spectral mixture analysis (MESMA) to determine the ground cover components. These methods assume that overall surface reflectance can be modeled as “a combination of the spectra of separable ground components”, and that the total sum of the various spectra equals the actual fractional cover on site (Ray & Murray 1996; Settle & Drake 1993 cited in Meyer and Okin 2015, pp. 123).

Some have sought to take advantage of the increasingly availability of HR satellite imagery to use methods that harness the potential of increased spatial resolution. (Malatesta et al. 2013) for example, used HR Rapid-eye 5m resolution satellite images and image classification (Maximum Likelihood classification) to map vegetation in Yemen through the use of spectral signatures from different plant species to augment the classification

Cao. et al. (2018) used HR satellite image to estimate the age of encroaching shrubs in the arid/semi-arid grasslands.

Other applications include but are not limited to evaluating the productivity of rangeland, mapping invasive species, monitoring vegetation and soil moisture, and monitoring and mapping fire extent (Al-Bukhari, Hallett, and Brewer 2018: 6-9).

The critical requirement among all these studies were the spatial resolution or effective pixel size of the satellite imagery, one of the three resolutions of satellite imagery sources discussed in the previous section.

Although regional rangeland assessments typically use coarse spatial imagery like Moderate Resolution Imaging Spectroradiometer (MODIS) (>250m spatial resolution); Advanced Very-High Resolution Radiometer (AVHRR) (1km² spatial resolution); or Landsat (30m spatial resolution), these imagery sources have their uses in providing broad level characterization but when looking at specific regions, could be associated with lower accuracy of the extracted quantitative measurements (Al-Bukhari, Hallett, and Brewer 2018: 6)

For monitoring and characterization of landscapes at a more detailed level, the spatial resolution needs to be smaller than the “scale of variability” of one of the dominant landscape types (Okin and Roberts 2004: 2). Introducing High resolution satellite imagery like WorldView (sub-meter resolution), Quickbird, and IKONOS for the detection of weeds and measurement of sagebrush-steppe for example yielded high overall accuracy and better detection in variation of shrub cover which demonstrates the material benefits of high-resolution imagery (Sant et al. 2014 cited in (Al-Bukhari, Hallett, and Brewer 2018: 6)

Similarly, the use of a high-resolution Pleiades imagery (pansharpened 0.5m) in this study demonstrates the benefits of HR satellite imagery for mapping our object of interest.

3.2.3 Using other remote sensing dataset to augment Satellite Imagery

As mentioned earlier, in addition to space-borne satellite imagery, the availability of alternatives of other RS data sources (including aerial imagery or aerial LiDAR) means that the former can be augmented with observations from other RS platforms

Studies that have combined more than one type of RS dataset base their choice mainly on their object of interest, as well as the environment in which their object of interest is situated in.

Studies that have combined a coarser-resolution satellite imagery with a higher-resolution imagery (most commonly airborne imagery) include Olsson, Van Leeuwen & March (2011); Alexandridis et al. (2017), Marshall, Lewis & Ostendorf (2014), Sandino et al. (2018) for the purpose of detecting weed infestation, with Sandino et al. (2018) also employing ML for that purpose.

The most common addition is aerial imagery from a UAV which helps to augment the spatial resolution (or ground sampling distance) up to 0.01m to act as ground-truth or to monitor specific areas of interest within the extent of the satellite imagery. Examples of these studies include:

1. Comparison of machine learning classification methods to classify desert vegetation, as Al-Ali et al. has done so in the Kuwaiti desert (Al-Ali et al. 2020).
2. for the purpose of classifying estuarine environments using ML (Gray et al. 2018)
3. Drone imagery segmentation using machine and deep learning for mapping bog vegetation communities*** (Bhatnagar, Gill, and Ghosh 2020)
4. UAV multispectral imagery w sat imagery for monitoring forest health (Dash, Pearse, and Watt 2018)
5. Detailed landscape analysis by UAV for post-mining sites in Indonesia compared to satellite imagery (Iizuka et al. 2018)
6. UAV and ML to detect invasive buffel grass in Cape Range National Park WA (Sandino et al. 2018)

Before a study-area wide analysis of RS imagery can take place, it often needs to be classified in order to quantify the spatial relations of the various objects present in the imagery. Imagery that is not classified will not yield much information and insights for the RS user.

3.3 Image Classification Approaches

Image classification is a mainstay of remote-sensing research projects and studies because the RS user needs to know what are the real-life objects in the data representation- the raster image composed of millions of pixels- to quantify its corresponding characteristics and ascribe changes (if any) over space-time or at a single point in time.

The process of classification however may be difficult due to the inherent complexity of the landscape in the study area or process-related challenges arising due to the selection of the satellite image (e.g., unsuitable satellite imagery with regards to spectral, radiometric, spatial or temporal resolutions), selection of classification method, or selection of training samples, (Lu and Weng 2007)

The classification of certain scenes for example, is much more complex in practice. In Australia, the "Outback" in colloquial term, make up a major part of the Australian continent,

states, and territories notwithstanding. Its arid environment generally comprised of low open woodlands and shrublands with a heterogeneity due its low vegetation cover; spectral similarity between non-photosynthetic vegetation (the majority of vegetation in the desert) and bare soil, shadowing and multiple scattering which proves a challenge for analysts of satellite images to discern the components and objects in the scene (Qi et al. 1994; Huete et al. 2002). Arid vegetation also lacks a distinct red-edge compared to its humid counterpart which adds to another challenge in detecting vegetation in the arid environment.

Going beyond mapping vegetation and non-vegetation into mapping specific species of vegetation is even more challenging without additional augmentation methods to distinguish between various species of vegetation in an environment dominated by brown vegetation and bare soil. The complexities however, have not deterred remote sensing analysts in trying to overcome the challenges listed above, and in that process have spawned a gamut of methods in response to the aforementioned challenges.

Lu and Weng (2007: 830) have summarised a taxonomy of classification methods based on various categories including supervised vs unsupervised; parametric vs non-parametric; per-pixel vs sub-pixel; object-oriented vs per-field; hard vs soft (fuzzy) classification; spectral vs contextual as well as the various algorithms that accompany the classification methods. All-in-all, there were over 50 kinds of classification methods with various permutations due to the open plug-and-play approach for image classification processing.

This literature review limits discussion to the four types of classification methods used for the dataset.

3.3.1 Pixel-based Methods

Unsupervised Pixel-based Classification

Unsupervised Pixel-based classification methods do not involve contextual knowledge provided by the RS analyst, nor derive any contextual knowledge from the imagery itself except for the statistical distribution of the spectral characteristics of the pixels (Lu and Weng

2007: 830). It is a “pure” classification process of assigning each pixel into classes. Because it is unsupervised, “clustering-based” algorithms stratify the pixels into various classes based on statistical information of the digital number (pixel value). Thus, the higher the radiometric resolution and wider number of spectral bands the better the classification result will be. Once the values are classified into ‘bins’, the RS analyst may merge the classes and apply the class labels to the bins.

Although it normally functions as a single-pixel classifier, take for instance, ESRI’s Unsupervised Pixel-based Classification tool (ESRI Inc. 2020), there are sub-pixel tools available in the commercial market too¹, especially for moderate-resolution satellite imagery with pixels that have a high proportion of mixed pixels. As opposed to a “pure” pixel which represents only one spectrally homogenous object, a “mixed” pixel represents a mixture of objects that is mixed into one pixel. The former is relatively easy to classify by a machine by simply matching its profile with its spectral signature while the latter requires more complex techniques like fuzzy classification and spectral mixture analysis (SMA) to determine its components (Li et al. 2014: 390).

SMA is the most common (as well as effective) pre-classification analysis step for mixed pixels classification (Lu and Weng 2007: 837). SMA works with multispectral imagery because the various bands (3 to 10 bands), Red, Green, Blue, Near Infrared (NIR), Short-waved Infrared (SWIR1 &2), Thermal Infrared (TIRS1 &2) will be able to better reflect the different reflectance from different materials and discriminate different vegetation down to species level and its health.

Some studies that rely on SMA to classify moderate-resolution satellite imagery include:

1. Fractional Cover in Western Kalahari-Savanna environment, using SMA on MODIS to retrieve PV, NPV, and Soil validating with vegetation transects (Meyer and Okin 2015)

¹ ERDAS Imagine, a commercial RS software has a subpixel classifier

2. Tree cover in semi-arid woodlands (pinyon juniper)- comparison of vegetation indices and SMA for detecting tree cover using Landsat TM and 1m NAIP for validation (Yang, Weisberg, and Bristow 2012)
3. Monitoring of dryland woody plant dynamics with the use of vegetation indices or spectral mixing analysis to account for the “fine-scale” heterogeneity of vegetation and soil in arid landscapes (Yang et al. 2012, pp. 63)

Although with relatively good accuracy rates (Fisk, Clarke, and Lewis 2019), it requires a specialized hyperspectral sensor for the remote sensing equipment (e.g., satellite or airborne aircraft) which can be costly or not easily accessible.

Supervised Pixel-based classification

Supervised pixel-based classification’s main differentiating factor from the unsupervised method is its use of user-input spectral signatures to collect spectral signature for each class from the input raster (Lu and Weng 2007: 830). Like unsupervised pixel-based classification, neighbouring pixels would not be taken into consideration, but signatures generated from training samples are used to train the classifier. Maximum Likelihood classifiers for example, are used in ESRI’s supervised classification tool. Because it is a parametric classifier, it assumes a normal distribution of the pixel values and distributes them into the classes based on the statistical distribution. This means that the quantity of samples collected need to be similar in order to avoid introducing selection bias into the classifier. It is also important to collect adequate training samples to avoid the “Hughes effect” which describes a drop in performance of the classifier when there are not enough training samples relative to the number of features used in the classifier (Richards 2013: 386). In some cases, the satellite imagery needs to be simplified (e.g. reduction of spectral bands, reduction of radiometric depth).

3.3.2 The move towards Object-based Methods

Given that hyperspectral tools might not be available due to its cost, and pixel-based analysis could only produce pixel-based outputs and general cover, there was a shift towards object-based image analysis (OBIA) through “delineating and analysing image-objects rather than individual pixels” (Castilla and Hay 2008; Blaschke 2010 cited in (Chen et al. 2018: 159). This shift came in tandem with the increased availability of high-resolution satellite imagery as more satellites were launched in the early 2000s. (Chen et al. 2018: 160)).

The shift from pixel-based to image-based represents a leap in capabilities because it produces meaning beyond a “technically defined unit”, the pixel by situating an object of interest in the image and drawing from it, inferences, and characterisation of a spatial nature (Blaschke, Lang, and Hay 2008: 13). By drawing deeper contextual information, we can create better quality maps through finer-resolution object classification beyond the pixels. These better-quality maps, with enough geo-accuracy, can be used for a multitude of purposes including but not limited to resource management; aiding decision-making in conservation efforts; carbon accounting; disaster management; biodiversity monitoring; and detecting change (including urban changes) all of which requires the identification of image-object and its shape boundaries and measuring any changes to its boundaries or characteristics within those boundaries.

This allows OBIA to imbue human-provided contextual knowledge and fuse with a machine’s computational power which is more powerful for analysis than assigning a class (or multiple classes) to a pixel representation which only clarifies what the object is behind the pixel unit.

Object-oriented classifiers- Image Segmentation using Support Vector Machine (SVM)

A popular method of object-oriented classification is image segmentation which is available in ESRI’s ArcGIS Pro as well as Trimble’s eCognition software (ESRI Inc. 2020; Trimble Inc. 2021) . The starting point is pixel-based as it groups pixels it thinks as belonging to an object

in order to form a feature-object². Chen et al. (2018). While a parametric classifier (Maximum Likelihood) was used in the supervised pixel-based classification method in ArcGIS Pro (ESRI 2020b). Segmentation was done using a non-parametric classifier (SVM)^r which allows its parameters to remain constant regardless of the number of samples used in training and could produce better predictions. As statistical information of the image is not used to classify the pixels into various segments, other data apart from spectral data can be used to segment the various pixels into meaningful segments. The segmentation process groups pixels into shapes according to an algorithm that is defined by the user, most commonly its “texture, colour, shape, size and grey levels” (Lucchese and Mitray 2001 cited in (Hossain and Chen 2019: 116)

There are various approaches to carry out segmentation, namely edge-based, region-based, hybrid methods, and semantic methods. Edge-based methods detects the contours of an object by a sudden change in pixel properties; region-based methods start from the centre of an object and starts incorporating similar type pixels to merge until it decides that there are no similar adjoining pixels in the neighbourhood; hybrid method which uses the former to detect edges and then the latter to merge the objects; and semantic methods which employ Machine Learning algorithms that approximate from the large number of training datasets that is labelled the object of interest by humans (Hossain and Chen 2019: 122).

The segmented image is then used to train the classifier (using one of the following algorithms: Maximum Likelihood, Support Vector Machine or Random Trees) using features like average chromaticity colour, count of pixels, compactness, or rectangularity, producing a Classifier Definition File (.ecd file) with its final output, classified features as an overlay over the raster image (ESRI 2021d).

Hossain and Chen (2019) noted a few key challenges associated with the object-based segmentation methods. While pixels within an individual object display high spectral

² Also referred to as “geo-object” in some other papers (Wu et al. 2021)

autocorrelation, objects have an intrinsic scale, hierarchical structure, and are composed of structurally associated parts, properties which need to be considered during segmentation. When many trees make up a forest, the forest can be contextualised better at a coarser resolution rather than at a finer resolution where individual trees can be discerned. On the other hand, if the object is an individual tree, then it is better to segment that object at a finer resolution where individual trees can be discerned.

While the Segmentation method in ArcGIS Pro 2.8 uses a linear classifier like Support Vector Machine (SVM) to linearly separate distinct classes using support vectors and separation hyperplane with lesser samples needed compared to Maximum Likelihood Classifiers or Deep Learning classifiers. Training attributes could include scale, shape, compactness, or smoothness for the segmenting process³ (Huang et al. 2020: 3463).

Because of its wide utility and standing as one of the more important classification methods, there are a few modelling frameworks introduced for varying classification purposes. The standard segmentation framework consists of: segmentation- feature extraction- classification (in that particular order). There are however, other frameworks that exist including multi-step classification, where classification results from a segmentation at a coarser scale is used to refine segmentation process at a finer scale; as well as preliminary classification by using the characteristics of an adjacent neighbour to the studied object (Eckert et al. 2017; Guo, Zhou, and Zhu 2013 cited in (Chen et al. 2018: 170).

In a study at a national park in Western Australia, Sandino et al. (2018) employed a straightforward standard segmentation framework (figure 8) to map invasive grass. The framework (see figure below) involves image acquisition, pre-processing of the image, image labelling (of the 6 classes), feeding these samples totalling 85,657 pixels into a XGBoost

³ In ESRI's Image Segmentation tool for training the SVM classifier, Converged Colours, Mean Digital Numbers, Standard Deviation, Pixel Count, Compactness and Rectangularity are some of the attributes used for training the classifier.

classifier (Decision Tree Model), and through the classifier, producing a segmented image with a detection rate over 95% for invasive grass.



Figure 8- Extracted from 'UAVs and Machine Learning Revolutionising Invasive Grass and Vegetation Surveys in Remote Arid Lands' (Sandino et al. 2018)

3.3.3 The step towards multilayered classifiers- Deep Learning Convolutional Neural Networks

Deep Learning has started trending again in recent years because of its varied applications to complex tasks but Convolutional Neural Network (CNN), in its earlier conception as Artificial Neural Network (ANN) has always demonstrated high potential for a powerful image classification algorithm classifier (Vaidya and Paunwala 2019: 55). CNN however, evolved in its capabilities with the availability of large quantity of datasets and better computing power from faster Graphics Processing Units (GPUs) (Vaidya and Paunwala 2019: 55).

In Deep Learning, the feature extraction process is more complex with layers and layers of convolutional and pooling layers (as opposed to a single layer classifier in SVM) that learn from examples and solves the issues of identifying relevant features for image classification as a multi-parameter optimization problem (Kumar, Upadhyay, and Kumar 2020: 34). Vis-à-vis SVM, Deep Learning requires more labelled image samples for training to find a well-fitting model for classifying the image. Because of its multilayer structure, DL frameworks like

Convolutional Neural network, as its name suggests, works similarly to a human brain in image, language, and speech recognition tasks compared to traditional classifiers with shallow layers (Chen, Lin et al. 2014 cited in (Yue et al. 2015: 469)

CNN Architectures

Behind the design of the CNN is a complex set of code (or architectures) complete with mathematical algorithms that assists with the tasks at hand. Some examples of CNN architectures used for image classification tasks include LeNet-5, AlexNet, VGGNet, GoogleNet, ZFNet and ResNet (Vaidya and Paunwala 2019: 69). ResNet was introduced in 2015 and had the least error rates in a comparison study of the listed architectures on an ImageNet dataset (Vaidya and Paunwala 2019: 69). It was revolutionary for its optimization in spite of its 152 layers by overcoming a potential over-fitting problem with learned layers from shallower models (Vaidya and Paunwala 2019: 67).

For the classifier to work properly, the dimensionality of the dataset often needs to be reduced to avoid the “Hughes effect” mentioned earlier under pixel-based classification but is also a concern for machine-learning classifiers (Maxwell, Warner, and Fang 2018: 2802). This would be relevant for the Pleiades imagery used in this study as it is a 4-band multispectral image and subsequently reduced to 3-band for the purpose of classification, as most CNN classifiers only work with three dimensional datasets.

To overcome the “Hughes effect” with regards to quantity of training samples, a pre-trained ResNet with 34 layers instead of the original 152 was used as the backbone model with transfer learning to ensure that a pre-trained CNN can be used on another set of data without the need to train the model from scratch. This overcomes the limitations of a smaller training dataset when data acquisition is limited or in the absence of big data (Hu et al. 2015: 14682)

Key Points

From a summary of the literature on remote sensing, vegetation mapping in the arid environment, and classification methods, it is apparent that Sandino et al. (2018: 2)'s axiom that there is no one-size-fits-all approach largely rings true.

There are however, important considerations for various steps of a classification process:

1. Spectral and spatial characteristics of the object of interest to be analysed;
2. Choice of primary imagery source (and secondary source if necessary to augment the first) determined by the requirements across the four types of resolutions;
3. Pre-processing requirements for input into the classification software and its fidelity to its original format;
4. Classification methods suitability to objective and object of interest;
5. General performance of classifiers and their associated algorithms

These considerations were referred to in the methodology used for this study.

4. METHODOLOGY

For the mapping segment, four classification methods were employed: a) Unsupervised ISO Pixel-based classification; b) Supervised Pixel-based classification- Maximum Likelihood (ML); c) Object-based Image Classification using segmentation- SVM; and d) Object Classification using Deep Learning- Convolutional Neural Network on Pleiades 0.5m pansharpened satellite imagery using ArcGIS Pro (ESRI Inc. 2020) to map 2 types of distribution in which Chenopod Shrubs present itself and make a detailed analysis and comparison of the benefits and drawbacks of each method.

Field work involved the collection of UAV imagery containing chenopod shrub communities (and other non-chenopod classes including ground and other vegetation classes) as training samples and validation and accuracy assessment. Field work was timed to be conducted during the winter months (where Pleiades imagery was captured a year earlier), which reduced the disparate effects of seasons on the variability of the landscape.

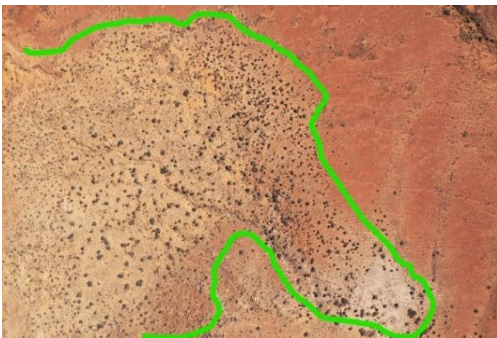
4.1 Mapping vegetation and Classification Schema

In this study, Chenopod Shrubs are the object of interest for their role as habitat for the TBGW and its links with population growth of the TBGW. As its habitat, the size of the plant and its density distribution are influential factors of its viability to support the proliferation of the TBGW.

Dense chenopod communities are especially suited to hosting birdlife than individual shrubs alone. Its state, and whether it is green and flowering chenopod shrubs also matters as they are a better source of food than senesced shrubs, which are barren.

Originally, four distinct patterns of distribution of chenopod shrubs were identified in the study area. They range from the smallest individual adult shrubs to two-three shrub-clusters to sparsely-distributed communities to dense chenopod communities. These distinct distributions can be discerned from the aerial photos taken by the UAV during field work over the study area. Original Classification Schema as documented in Table 1 below:

Table 1- Original Classification schema

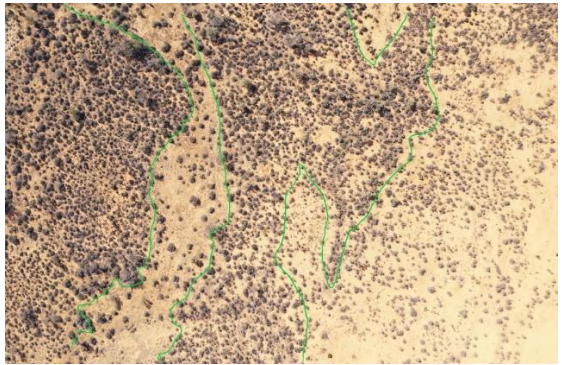
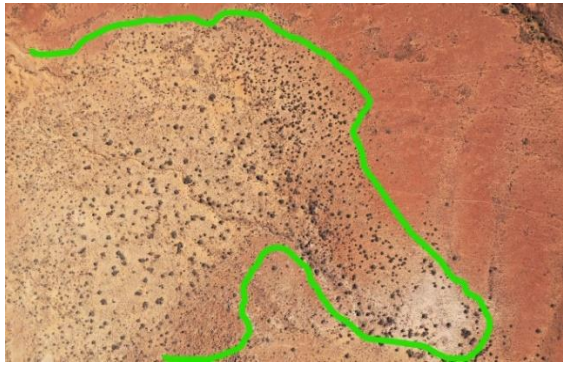
4 Classification Classes			
Individual Adult shrub 0.5m < Shrub width < 2m	Chenopod Communities <ul style="list-style-type: none"> • 2 or more shrubs combined • densely packed or sparsely distributed 		
Object Size & Spectral Variance Small → Large			
1. Individual Chenopod occurring on sandy build-up over a shale environment	2. Chenopod Communities comprising 3-4 shrubs	3. Dense Chenopod Communities comprising over 100 shrubs densely packed over large swaths	4. Chenopod Patches (large swaths of patches of Chenopod shrubs widely dispersed)
			
<i>Sub-Class 1 Individual Chenopod Shrub</i>		<i>Sub-Class 2- 2-3 Shrub Community</i>	
			
<i>Sub-Class 3-Dense Chenopod Communities</i>		<i>Sub-Class 4 Sparsely-distributed Chenopod Communities</i>	

Upon running preliminary segmentation with the above classification schema, it was noted that results were difficult to obtain for sub-class 1 and 2 due to the small number of pixels per segment. Individual shrubs, mostly measuring 0.3-1m in width could not be picked up by the segmentation tool because of the spatial resolution of the Pleiades imagery, with each pixel measuring 0.5m. This concurs with Poon (2007: 45) who commented that there needs to be a minimum of three pixels in order to make out the object from HR satellite imagery.

Running the segmentation with lesser than 80 pixels per segment would also not be ideal as it would generate a salt and pepper effect that is associated with pixel-based classification that contributes to inaccuracies from the classification process (De Jong et al. 2001; Van de Voorde et al. 2004; Campagnolo and Cerdeira 2007; Gao and Mas 2008 cited in Weih and Riggan 2010: 1).

Upon a reappraisal of the ecological value of individual shrubs and 2-3 shrub community vis-à-vis dense and sparsely distributed (dispersed) chenopod communities it was decided that the former two sub-classes be replaced, leaving just the latter two sub-classes which represent higher propensity to support the TBGW as its habitat. The classification schema was subsequently modified to the following in table 2 and table 4 below:

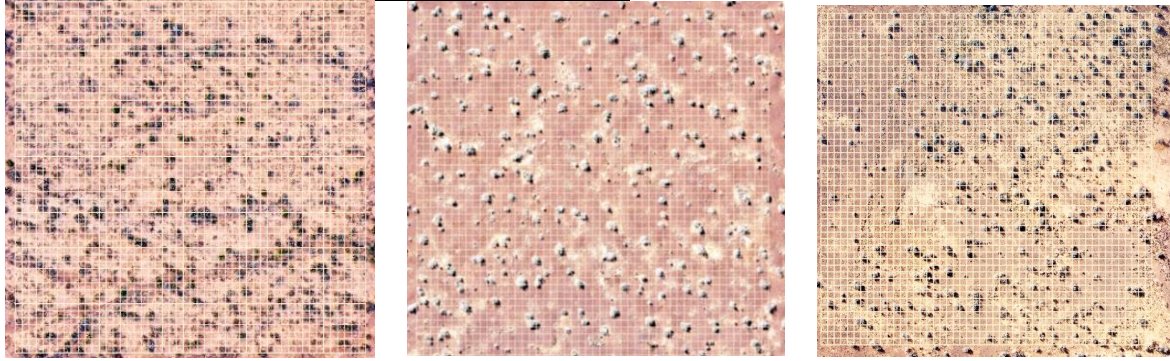
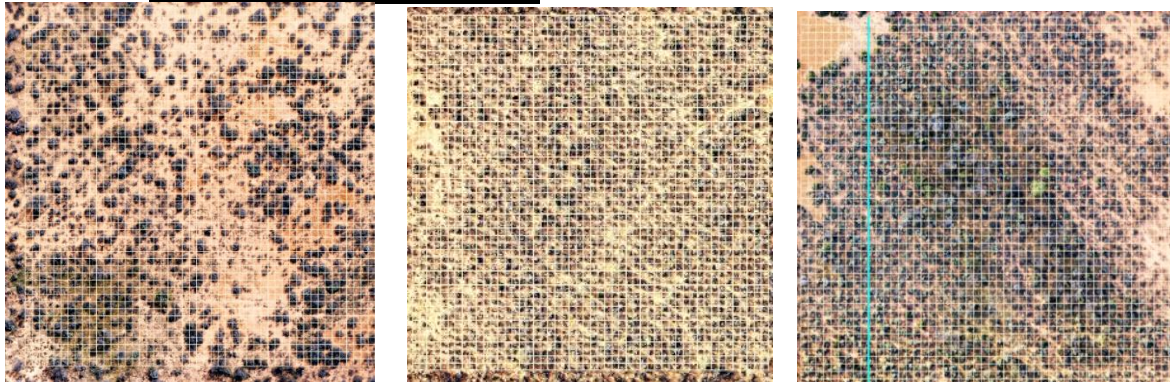
Table 2- Final classification schema- chenopod classes

<i>Class 1-Dense Chenopod Communities</i>	<i>Class 2 Sparsely-Distributed Chenopod Communities</i>
 	 

Original Sub-class 2, with communities consisting of 2-3 shrub classes was merged under dispersed chenopod community class 1.

A grid method was used to calculate the average density per 50X50m grid = 2500m² /0.25km²(25 hectares) by sampling three random areas over the UAV sample sites to derive the average chenopod density per hectare:

Table 3- Definition of chenopod classes by density of chenopod shrubs

<p>(i) <u>Dispersed Chenopod Communities Density Measurement= 7 shrubs/hectare or 700 shrubs/ km²</u></p>  <p><i>Fishnet 1- N= 164, Area 1E Fishnet 2- N=182 , Area 1F Fishnet 3- N=178 , Area 1D</i></p>
<p>(ii) <u>Dense Chenopod Communities Density Measurement = 20 shrubs/ hectare or 2000 shrubs/ km²</u></p>  <p><i>Fishnet 4- N= 334, Area 1C Fishnet 5- N=576, Area 1A Fishnet 6- N= 613 ,Area 1A</i></p>

The definition of sparse and dense chenopod communities are thus 7 shrubs per hectare and 20 shrubs and above per hectare respectively. In comparing the accuracies of the various classification methods for dense and dispersed chenopod community classes, these definitions were used to gauge the performance of the classification methods.

Other non-chenopod classes were also introduced in the classification schema to allow the machine to distinguish between chenopod shrubs and other photosynthetic plants like mallees and acacias as well as wide patches of bare soil, the former with its high NIR reflectance tends to be conflated with chenopod shrub communities and the latter which tends to drown out the reflectance of chenopod shrub communities especially for subclass (i). As a major vegetation

group classification class, they are the official NVIS classification schema, as MVG 22 (NVIS Technical Working Group 2017).

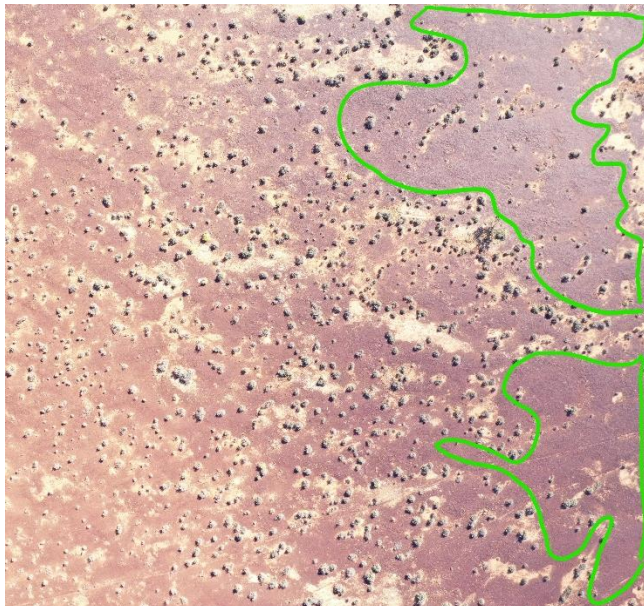
Other non-chenopod classes:

Table 4- Final Classification Schema- Non-chenopod classes

Acacia Open Woodlands class (non-chenopod vegetation class)



Shale class (Ground)



Bright Sand/ Clay Class- circled in green and Dark Sand Class- circled in blue (Ground)



4.2 Methodology Flow Chart

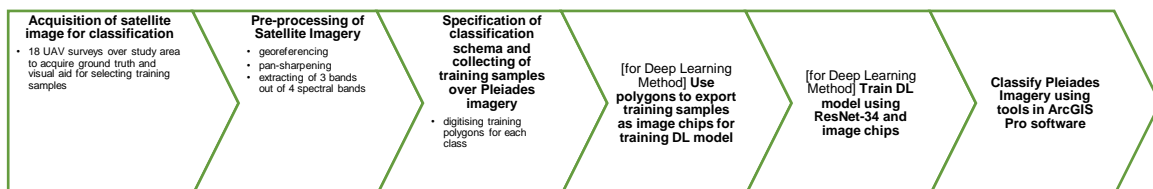


Figure 9- Classification flow-chart

4.3 Data Acquisition

4.3.1 Obtaining Pleiades Imagery of study area

Pleiades imagery was chosen for this study with primary consideration towards its high spatial resolution property. For this study which compares pixel-based and object-based classification methods, out of the four different resolutions mentioned earlier in the literature review, spatial resolution is of the utmost importance (followed by spectral, radiometric, and then temporal resolution), as it provides contextual information to the classifiers.

Pleiades imagery meets the requirements of the project and was thus chosen for the classification process for its costs and adequate specifications.

Original Pleiades imagery over study area was purchased from Airbus using an academic license. A panchromatic (P) TIFF file and multispectral (MS) TIFF file was provided with the following specifications:

Table 5- Processing level of Pleiades imagery ordered from Airbus

Processing level	Ortho -Corrected from acquisition and terrain off-nadir effects -Radiometric and Geometric adjustments
Date of Acquisition	19 June 2020
Time of Acquisition	01:01 GMT / 10:30AM
Geodetic Datum	WGS84
Projection	UTM 53S
Radiometric Processing	Reflectance
Cloud Cover	0%

Table 6- Pixel Values (Digital Numbers) Statistics of Pleiades Imagery

	Min	Max	Mean	Median	Std Dev
a) MS	0				
-Band 1 (B)		7506	2306.334	2387	660.303
-Band 2 (G)		5579	1593.579	1636	439.157
-Band 3 (R)		4139	1107.880	1134	295.390
-Band 4 (NIR)		7857	2656.453	2772	740.866
b) Pan-Chromatic	0	7949	2119.275	2186	619.380
c) Pan-sharpened image using GS method	0	4228 5855 7994 8191	957.0868 1377.122 1993.07 2294.66	-	468.534 684.321 1009.159 1149.65

4.3.2 Pre-calibration of Pleiades Imagery

Pansharpening

A 2m Pan-sharpened image was obtained from the 12-bit 4 Bands MS resampled and pansharpened with the 0.5m panchromatic image.

Rationale for pan-sharpening:

Nagendra (2001) recommended that pixel size of the satellite imagery be $\frac{1}{4}$ - $\frac{1}{3}$ the size of the scene or vegetation being mapped. Meyer et al. (1996) were less prescriptive and opined that the ideal spatial resolution depends on the size of the object and needs to be fine enough to discern the outline of the object, allowing maximisation of between-object variance while coarse enough so that the within-object variance (components of the object) is minimised and cannot be distinguished (Meyera et al. 1996 cited in Nagendra 2001: 2379). By pan-sharpening the Pleiades imagery from 2m to 0.5m, each individual adult chenopod shrub can be identified with chenopod communities even more identifiable within the context of neighbouring pixels.

Original Pleiades multi-spectral satellite image with 2m resolution were fused with its panchromatic counterpart 0.5m to produce a pan-sharpened image with the resolution of the latter. Traditional methods of pan-sharpening although benefits the spatial resolution of the imagery, do “alter the spectral integrity” of the data, thus it is important to pick a suitable pan-sharpening method (Laben and Brower 2000: 1; Jones et al. 2020).

Gram-Schmidt pan-sharpening was used in ArcGIS Pro to pan-sharpened the image (ESRI Inc. 2020). Gram-Schmidt was chosen as it often preferred by RS practitioners as it can process MS imagery with more than 3 spectral bands, less computationally intensive than other pan-sharpening methods, while minimising spectral distortions compared to other methods (Zhou et al. 2008 cited in Jones et al. 2020: 4).

Radiometric and spectral calibration for Object-based Image Classification- SVM and Object classification using deep learning

As ArcGIS Pro's Segmentation tool and DL tool only works on an 8-bit, 3-band raster image, Green (Band 2), Red (Band 3) and NIR (Band 4) bands were extracted in preparation for the segmentation-based classification process and the classification by deep learning process.

The blue band was left out as its spectral response for vegetation is often similar to that of the green band.

After the image was pan-sharpened and resampled to a 3-band image, the pixel value range across the three bands were similar to each other thus, no statistical normalisation of the pixel values was required prior to classification by the software.

4.3.3 18 UAV surveys over study area from 5th-7th August 2021

18 UAV surveys were conducted over the 80km² study area. The purpose of the UAV survey was to:

- (i) act as ground-truth for the satellite imagery;
- (ii) to form in-situ knowledge about the study area;
- (iii) guide the drawing of sample polygons over the Pleiades satellite imagery for the image classification process;
- (iv) provide accuracy assessments for the image classification methods

Each survey area was flown at height of 120m over 260m X 524 m, with a Ground Sampling Distance of 0.03m. Photos were taken at 75% frontal overlaps and 60% side overlap as recommended by pix4D (pix4D 2021a).

Camera: Hasselblad L1D-20c_10.3_5472x3648

Survey Areas were chosen to reflect the diverse landforms where chenopods can be found in the study area (see figure 17). These are namely:

- a) Gilgai Plains – a depression in the soil surface with cracking exposed clay plains
- b) Gilgai Plains- a depression in the soil surface with stony shale plains
- c) Drainage lines and floodplains which host up to 3 vegetation communities including Woodland (taller gum trees and Mulga); Shrubland; and Grassland over mixed chenopods

(Department for Environment and Heritage 2009: 16)

The 18 survey areas covered below covers 3.765 km² or 5.4% of the total study area.

Table 7- Details of each survey area

Flight Surveys and Scene Description	Date	Way point	Average GSD (cm)	Area Covered (km ²)	GCP Points
4D- Shale and Bright Sandy background with dispersed chenopod communities	5/08/21	87 (2 discarded)	2.76	0.200	4
4C Sandy background with dispersed chenopod communities and acacia open woodlands	5/08/21	89	2.9	0.212	Nil
4B Shale and Bright Sandy background with dispersed chenopod communities and acacia open woodlands	5/08/21	89	2.82	0.201	Nil
5A Shale and Bright Sandy background with dispersed chenopod communities and acacia open woodlands	5/08/21	88	2.81	0.209	Nil
5D Dark Sand, Shale and Bright Sandy background with dispersed chenopod communities and dense chenopod communities	5/08/21	88	2.88	0.215	Nil
4E Dark Sand, Shale and Bright Sandy background with dispersed chenopod communities and dense chenopod communities	6/08/21	80	3.01	0.220	2
4F Dark Sand, Shale and Bright Sandy background with dispersed chenopod communities	6/08/21	92	2.75	0.213	2
4G Dark Sand, Shale and Bright Sandy background with dispersed chenopod communities	6/08/21	78	2.82	0.186	2
1E Dark Sand Shale and Bright Sandy background with	6/08/21	86	2.89	0.214	2

dispersed chenopod communities					
1F Dark Sand, Bright Sandy background with dispersed chenopod communities and dense chenopod communities	6/08/21	84	2.88	0.205	2
1A Dark Sand, Bright Sandy background with dispersed chenopod communities and dense chenopod communities	6/08/21	88	2.99	0.224	2
1D Dark Sand, Bright Sandy background chenopod communities and dense chenopod with dispersed communities and acacia open woodlands	6/08/21	89	2.99	0.224	2
1B. Dark Sand, Bright Sandy Background, and Dense Chenopod communities	7/08/21	88	2.88	0.204	2
1C Dispersed and Dense chenopod communities	7/08/21	90	2.89	0.208	2
2A Dispersed and Dense chenopod communities with Acacia open woodlands	7/08/21	88	2.92	0.218	2
2D Dispersed and Dense chenopod communities with woodlands Acacia open	7/08/21	88	2.67	0.185	2
2B Dispersed and Dense chenopod communities with Acacia open woodlands	7/08/21	88	2.94	0.213	2
2C Dispersed and Dense chenopod communities with Acacia open woodlands	7/08/21	88	2.89	0.214	2

4.3.4 Processing Ortho-imagery in Pix4D

Processing options- Full Image Scale, using Geometrically Verified matching. The latter option helps to exclude image pair matches that are inconsistent. This helps in matching images that includes objects with similar features (e.g. crops, fences) which are prevalent in the areas to

be surveyed (pix4D 2021b). Images were pseudo-georeferenced with two GCPs for 2D orientation and scale.

Step 1: Initial Processing

Initial processing was done automatically by Pix4D software through “bundle block adjustment” which refers to the “bundle of light” analysed in each image translated from 2D to 3D projection using algorithms and collinearity equations (of image coordinates and altitude) from Pix4D to achieve true orthorectification (Burnham 2019: 8).

Processing Options



Detected Template	No Template Available
Keypoints Image Scale	Full, Image Scale: 1
Advanced: Matching Image Pairs	Aerial Grid or Corridor
Advanced: Matching Strategy	Use Geometrically Verified Matching: yes
Advanced: Keypoint Extraction	Targeted Number of Keypoints: Automatic
Advanced: Calibration	Calibration Method: Standard Internal Parameters Optimization: All prior External Parameters Optimization: All Rematch: Auto, yes

Figure 10- Initial Processing in Pix4D

Step 2: Point Cloud and Mesh

Processing Options



Image Scale	multiscale, 1/2 (Half image size, Default)
Point Density	Optimal
Minimum Number of Matches	3
3D Textured Mesh Generation	yes
3D Textured Mesh Settings:	Resolution: Medium Resolution (default) Color Balancing: no
LOD	Generated: no
Advanced: 3D Textured Mesh Settings	Sample Density Divider: 1
Advanced: Image Groups	group1
Advanced: Use Processing Area	yes
Advanced: Use Annotations	yes

Figure 11- Point Cloud densification in Pix4D

Step 3: DSM, Orthomosaic and Index

Processing Options



DSM and Orthomosaic Resolution	1 x GSD (2.76 [cm/pixel])
DSM Filters	Noise Filtering: yes Surface Smoothing: yes, Type: Sharp
Raster DSM	Generated: yes Method: Inverse Distance Weighting Merge Tiles: yes
Orthomosaic	Generated: yes Merge Tiles: yes GeoTIFF Without Transparency: no Google Maps Tiles and KML: no

Figure 12- DSM Processing Options in Pix4D. Note GSD is slightly different for each orthomosaic.

UAV Surveys 5th-7th August 2021

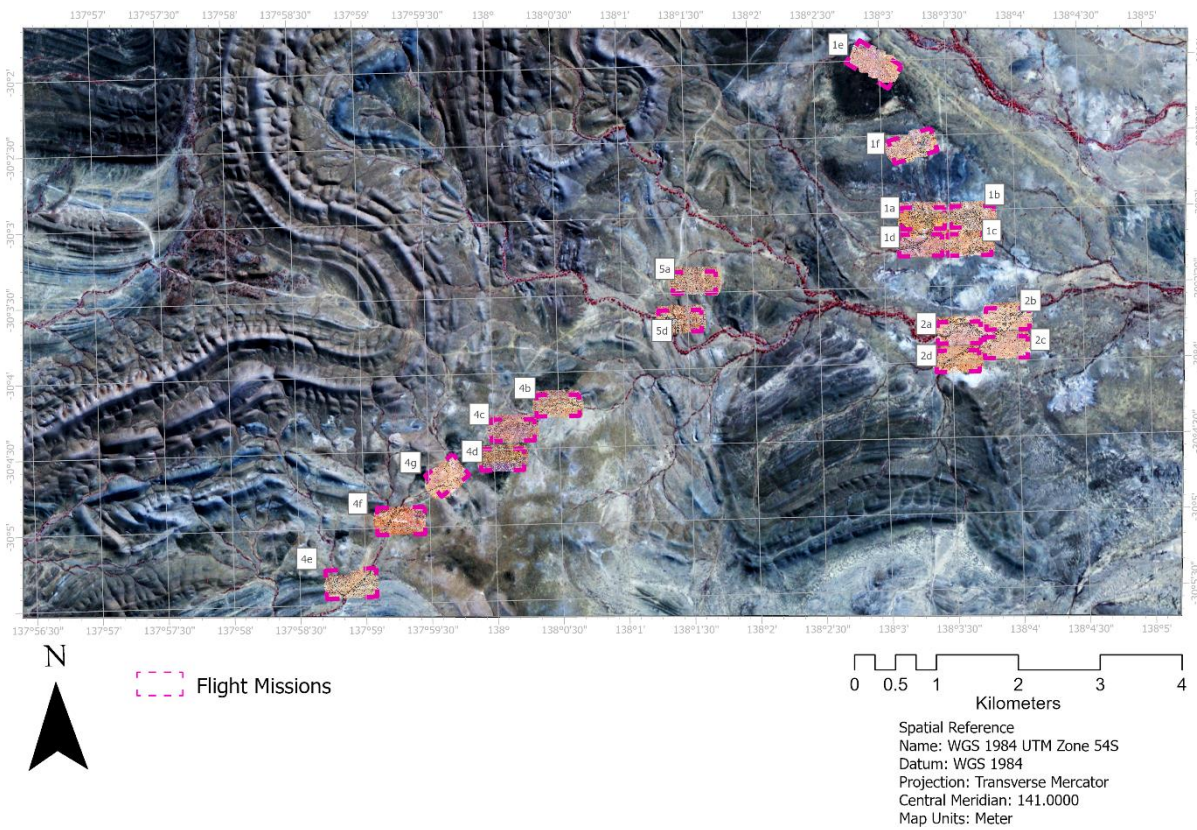


Figure 13- UAV surveys carried out at study area from 5th -7th August

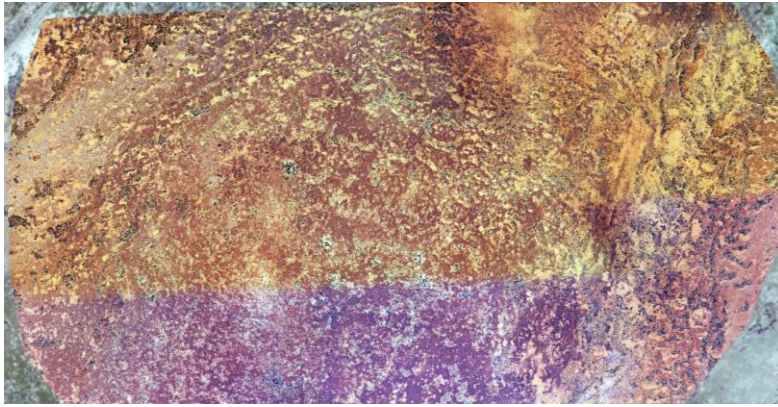


Figure 14- Area 4d

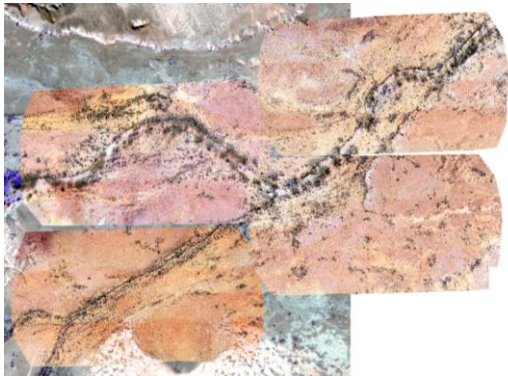


Figure 15- Area 2 (a,b,c,d)



Figure 16- Area 1 (a,b,c,d)

From the UAV surveys flown, it can be observed that chenopod shrubs present themselves on 3 types of background, namely Bright Sand/Clay, Shale, and Dark Sand as seen in figure 17:

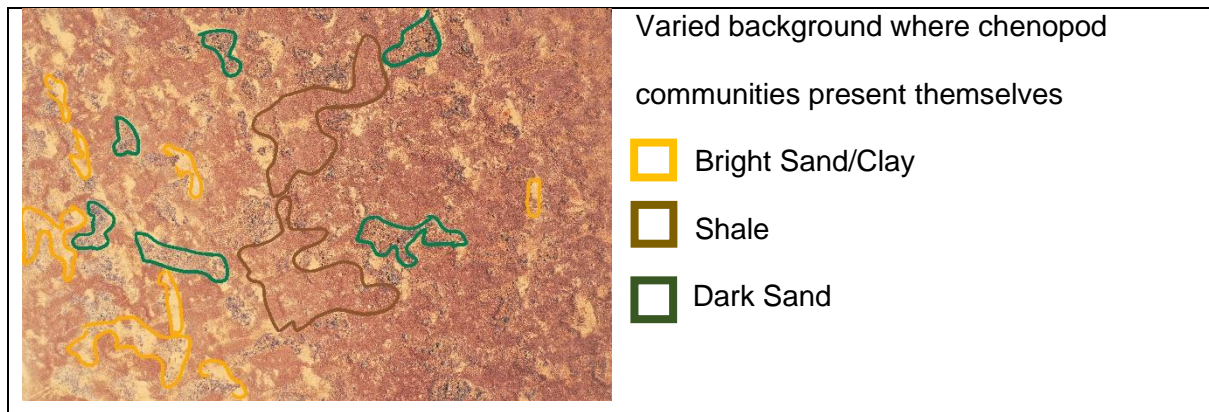


Figure 17-varied background where chenopod shrubs are present

4.4 Image Classification Tools

Image classification tools from the ArcGIS Pro software was processed on the pre-calibrated Pleiades Imagery that was clipped to the extent of the study area.

Polygon samples both for training and for a reference dataset for accuracy measurement were digitised manually, visually guided by the ortho-imagery collected from the UAV and used in the last three classification methods.

ISO vs Maximum Likelihood vs SVM vs CNN (resnet-34)

The four classification methods used four dissimilar algorithms which did the heavy lifting of the image classification work in either assigning each pixel to a class, grouping similar pixels to form objects, or identifying relevant features in an image which helps to classify image tiles across the entire study area.

The unsupervised Pixel-based tool uses an ISO classifier with k-means algorithm to partition the spectral image into spectral classes based on the overall statistics of the image (Lu and Weng 2007: 830). K-means clustering works on an iterative approach which links each observation with the nearest mean with the 'centroid' of each cluster becoming the new mean until a convergence is attained (ESRI 2021a).

The supervised pixel-based tool was processed using the Maximum Likelihood (ML) classifier which is based on Bayes theorem- it assumes a normal distribution for all samples in a class

and assign a class to each sample based on the highest probability. To avoid the “Hughes effect,” at least 100 samples were collected for each class, with a total of 837 samples taken for the 5 classes. (ESRI 2021b)

The object-based image classification tool was based on segmentation using SVM which groups similar pixels into various segments using a region-based approach⁴. It also requires lesser and less equally distributed samples compared to the Maximum Likelihood classifier and does not need the samples to be normally distributed. (ESRI 2021c)

The object classification using Deep Learning (DL) is based on a Convolutional Neural Network (CNN) which identify and rank features that are relevant to a class for image classification. It is pre-optimised with the ResNet architecture with 34 layers instead of the original 152 for training the DL model. ResNet is different from traditional CNN because it uses the residuals from each layer with reference to the layer inputs which helps to optimise the layers and gain higher accuracy (He et al. 2016: 770).

The tool was run twice, first using a larger image chip size and then a smaller image chip size. Only the accuracy results from the latter was retained for discussion as the performance for both training models were very similar and the latter will be able to present a classified result that is twice the resolution of the first attempt.

⁴ As mentioned in section 3.3.2, there are a few approaches to segmentation. A region-based approach starts from the centre of the object and incorporates similar-type pixels until it decides there are no more similar adjoining pixels in the neighbourhood.

4.4.1 Unsupervised ISO Pixel-based image classification

Unsupervised Classification was run on ArcGIS Pro (Esri Inc. 2020) with performs an unsupervised classification using ISO Cluster algorithm which groups the raster cells based on its spectral characteristics. A classification schema as delineated in section 4.1 was used to provide classes to label the separated spectral classes into semantically meaningful classes.

It has the least number of steps among all the methods because the software does the grouping of the pixels with the user only applying the class label to each group to form distinct classes.

4.4.2 Supervised Pixel-based image classification- Maximum Likelihood

The supervised version of the pixel-based tool also involves the use of the classification schema in addition to the use of spectral signatures collected from each class to train the Maximum Likelihood classifier.

The following samples were digitised and used to train the classifier:

Table 8- Samples for Supervised Pixel-Based Image Classification

Class	# Samples	Pixels (%)
Dispersed Chenopod Communities	193	6.46
Dense Chenopod Communities	128	3.46
Acacia Open Woodlands	77	0.73
Bright Sand/Clay	121	68.47
Dark Sand	106	5.81
Shale Ground	138	15.07
Total	763	

4.4.3 Object-based Image Classification using Support Vector Machine (SVM)

4.4.3.1 Segmentation Process

Removed due to copyright restriction

Figure 18- Object-oriented feature extraction workflow, extracted from (ESRI 2021)

The purpose of segmentation is to extract homogenous objects for vegetation mapping (Wu et al. 2021: 5). The segment mean-shift function groups similar adjacent pixels (controlled by spatial and spectral parameters decided by the user) into a contiguous segment. In ArcGIS Pro, it works only on 8-bits rasters (satellite image) with 1 or 3 bands. Before segmentation, the raster was pre-processed as in Section 4.3.2.

Image segmentation was carried out using the following parameters: Spectral Detail- 16.46; Spatial Detail- 8; Minimum Segment Size in Pixels- 80; Scale- 1: 1939 and mean-shift segmentation which group similar pixels (based firstly on spectral and then on spatial detail as determined in the parameters) with a minimum segment size of 80 pixels that could be 4.5 m wide segments that are suitable for classifying both dense and sparse chenopod shrub communities.

4.4.3.2 Managing Training Samples

The same training samples used for supervised pixel-base classification were used for this method:

Table 9- Samples for Segmentation using SVM

Class	# Samples	Pixels (%)
Dispersed Chenopod Communities	193	6.46
Dense Chenopod Communities	128	3.46
Acacia Open Woodlands	77	0.73
Bright Sand/Clay	121	68.47
Dark Sand	106	5.81
Shale Ground	138	15.07
Total	763	

A spectral profile was also generated for each class, looking at the mean reflectance value to see the difference in spectral response across the four bands (red, green, blue, and NIR) which also helps to inform the calibration of the spectral parameters of the segmentation tool. If spectral responses are similar between classes of interest, parameter for spectral details should be higher to better distinguish the two classes. In this case, as both dense and sparse chenopod classes had similar responses, the spectral parameter in the tool was kept at 16.46 (out of a maximum of 20).

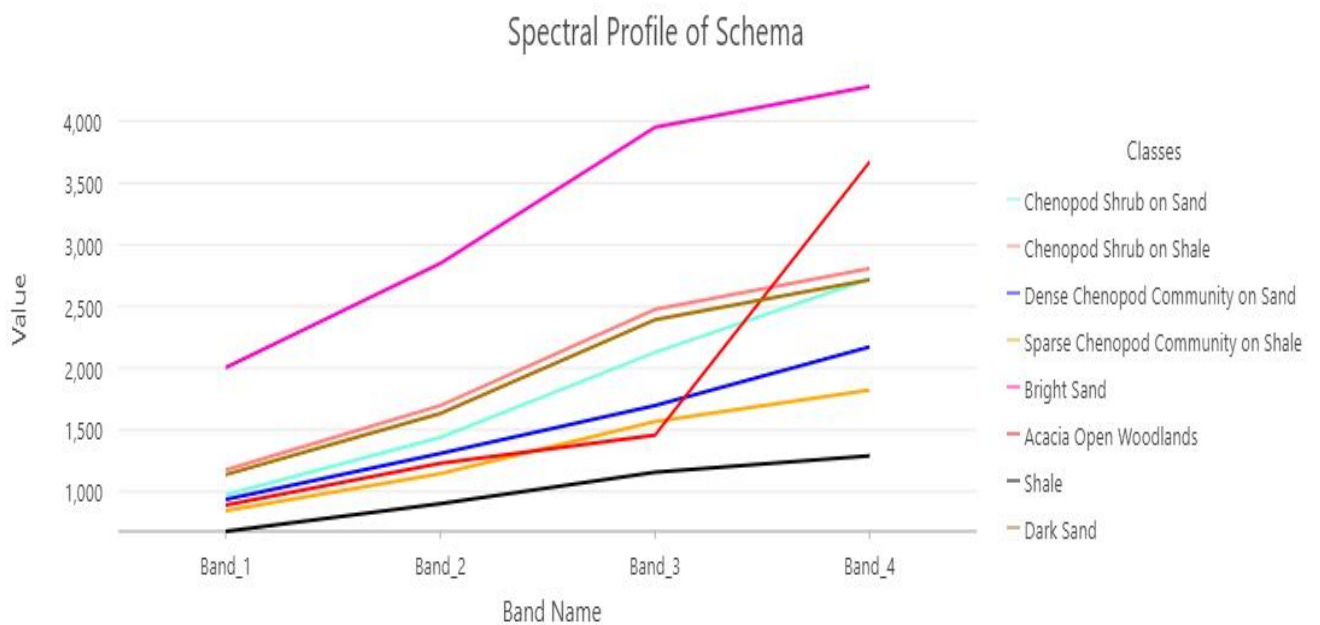


Figure 19-Spectral Profile of classes

The results of the segmentation are in section 5.3.

4.4.4 Object Classification using Deep Learning- Convolutional Neural Network (CNN)

4.3.4.1 Label Objects for Deep Learning

- Labelling objects for deep learning and exporting training samples

- Importing Top-level Schema informed by the NVIS Classification Scheme, followed by sub-groups pertains to the requirements of the research objective and the dataset
- Ensure minimum of 100 training samples per class

The first step for the classification processing using DL is the labelling of objects for training the model. It is recommended that the optimal training size for Deep Learning be 20% of the study area (69.34km²) which means 13.87 km² of samples should be collected. However, because of the sampling area was limited to the area covered by the UAV, a minimum of 100 samples (totalling 837 samples, amounting to 0.52 km²) were taken for each class. With a preconfigured training architecture and transfer learning however, the issue of the training size is ameliorated.

The previously segmented image helped in the selection of samples with segmented polygons and additional polygons digitised to help in the export of training samples for training the DL model

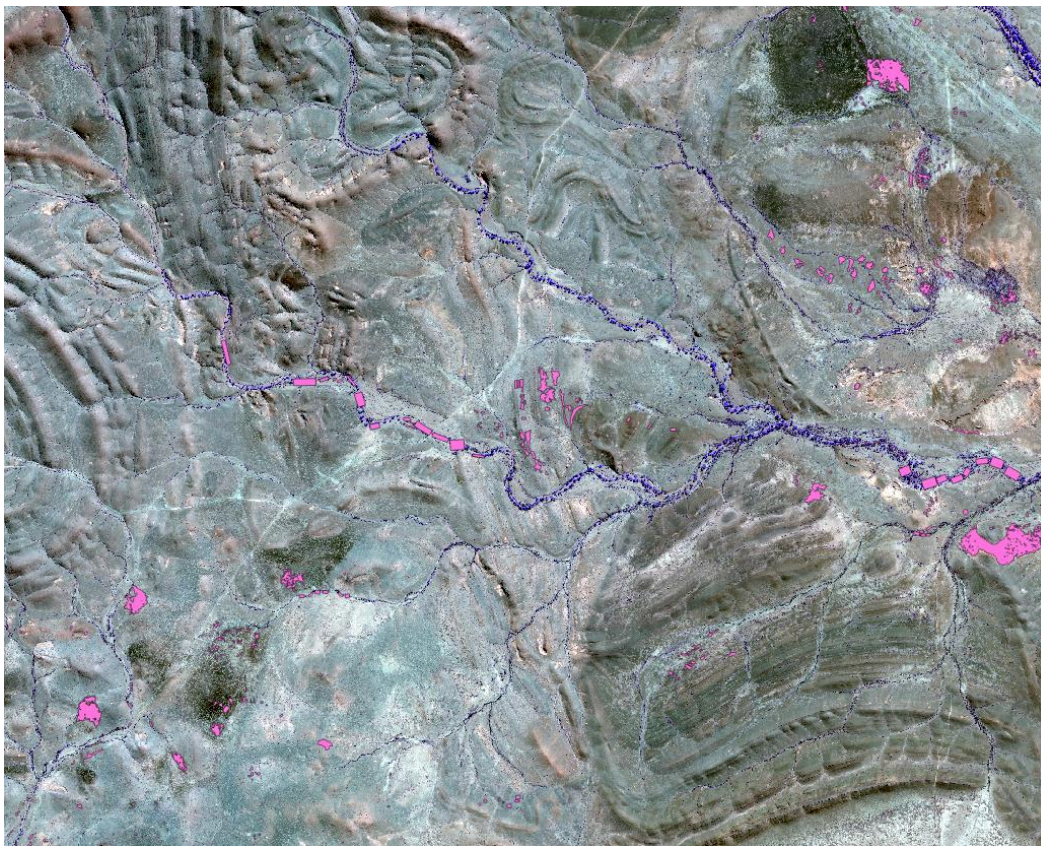


Figure 20- Distribution of training samples across study area

Table 10- Training Samples used for training the deep learning model

Class	# Samples	Total Area (km ²)
Dispersed Chenopod Communities	231	0.066990
Dense Chenopod Communities	130	0.028508
Acacia Open Woodlands	105	0.099717
Bright Sand/Clay	129	0.147642
Shale Ground	132	0.130678
Dark Sand	110	0.054131
Total	837	

4.3.4.2 Prepare Training Chips and Train Deep Learning Model

Table 11- Parameters of Training DL Model

Classify Objects using Deep Learning	Step 1: Export Training Data	Step 2: Training Deep Learning Model
Attempt 1 -ImgClassificationChip1 -ImgClassificationModel1 Processing extent- 4a/4b/4c/4d/4g/4g 5a/5d 1a/1b/1c/1d/1f 2a/2d	Tile Size (X, Y)- 128,128	Max Epoch 20
	Stride (X, Y)- 64,64	Model Type Feature Classifier
		Batch Size 64
	Effective Tile Size (m)- 64X64m	Chip_size* 108
	Number of Samples- 2617	Backbone Model resnet-34
		Validation- 10%
Attempt 2 -ImgClassificationChip2 -ImgClassificationModel2 Processing extent- 4a/4b/4c/4d/4g/4g 5a/5d 1a/1b/1c/1d/1f 2a/2d	Tile Size (X, Y) 64, 64	Max Epoch 20
	Stride (X, Y) 32,32	Model Type Feature Classifier
	Effective Tile Size (m ²)- 32X32m	Batch Size 64
		Chip_size* 54
	Number of Samples- 2617	Learning Rate
		Backbone Model resnet-34 Validation- 10%

Epoch was set at 20 to avoid overfitting of the data. This means the dataset gets passed through the neural network 20 times at most, with no more than 20 learning cycles. The

number of epochs should be relative to the size of the training set to avoid over-fitting (Courtial et al. 2020: 10) Over-fitting the data means that the model has learned how to solve the training data well but is not generalised enough to solve other classification needs.

Selecting the image tile size is one of the most important determinants of the model accuracy, as the image tile size gives specific context to the model. A smaller chip size magnifies minute details to the machine giving it as one of the options to include when selecting relevant features while a larger chip size can be used to obscure these minute details in favour of the larger context if the RS user deems the latter more relevant to the object of interest. Previous studies have shown that a calibration of the image chip size that preserves as much context as possible gives better results (Courtial et al. 2020: 14)

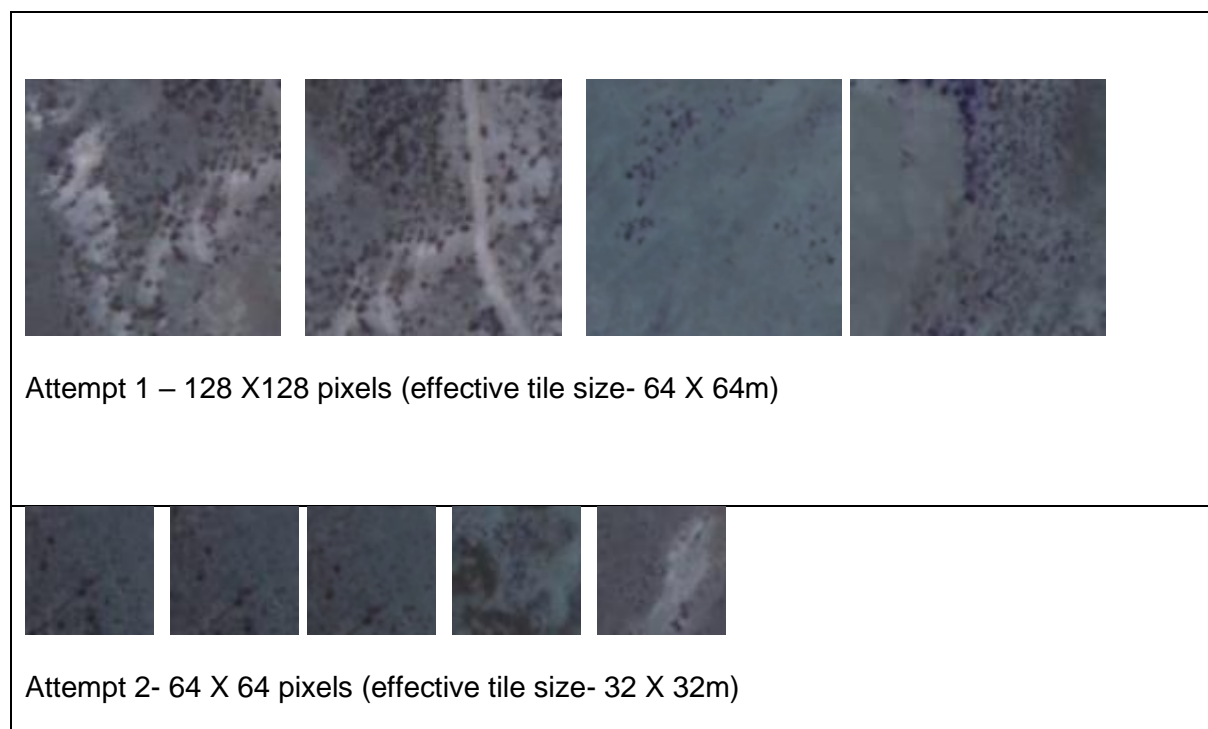


Figure 21- Sample Training Chips for both attempts

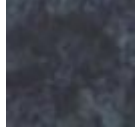
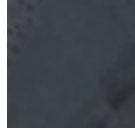
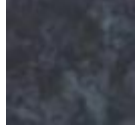
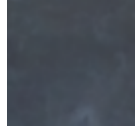
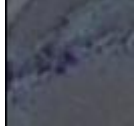
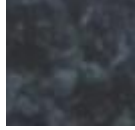
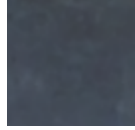
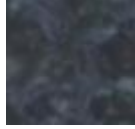
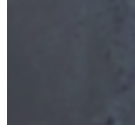
Dispersed Chenopod Communities	Dense Chenopod Communities	Acacia Open Woodlands	Bright Sand/Clay	Shale Ground	Dark Sand
					
					
					
					
					

Figure 22- Sample Training Chips according to labels (classes)

Training of the DL model is also done within ArcGIS Pro 2.8 (ESRI Inc 2020.) which makes the DL process more user-friendly. The training uses the image chips, 2617 chips for training the DL model with a preconfigured neural network with 34 layers (resnet-34) used as the backbone architecture. Transfer learning ensured that we did not have to train a neural network from scratch and that the 2617 training chips were sufficient for training a reliable model.

The training works by first identifying lower level features (e.g. edge) important for distinguishing between object, and then builds on these lower level feature to find the combination that are the most relevant for the class (Vaidya and Paunwala 2019: 56).

In the CNN, the input image goes through the convolution process that involves the multiplication of a set of weights with the input, iteratively selected during the training to

achieve desired output, to help select and identify these relevant features, back and forth through the CNN (Vaidya and Paunwala 2019: 58).

4.3.4.3 Classify Objects using Deep Learning Tool

Due to software limitations, the tool could only run at smaller extents each time, instead of the entire study area. The Classify Objects using DL Tool was run 10 times over areas surveyed during the field work from 5th -7th August. The results of the classified area are in section 5.4.2.

4.4.5 Measuring Accuracy of the results from the four methods

There are a few approaches to measuring accuracy in RS classification and (Richards et al. 2013: 396) noted four main ones: (i) Testing Set (or Accuracy Assessment Points); (ii) Error Matrix or Confusion Matrix; (iii) Kappa Coefficient; (iv) cross-validation accuracy assessment.

The first three accuracy assessment methods were used on all four classification methods while the last one was already in-built into the DL training model software tool. The cross-validation accuracy assessment involves excluding a subset of the training samples for validation purposes after the classification is done. In DL, 10% of the training samples were kept as validation samples to assess the model performance (or precision) and used to halt training once an equilibrium has been reached for the loss value (which refers to the predicted number of errors for a DL training model).

Classification accuracies are commonly tabulated in the confusion matrix which provides the user's accuracy and producer's accuracy that can be used to determine the overall accuracy.

In the software used for this study, the accuracy assessment tool is in-built in 2 out of the 4 classification tools used for this study- Supervised Pixel-based classification and Object-based Image Classification using segmentation. 500 accuracy assessment points were generated, randomly distributed across the classified area, and stratified (proportionate to the size of each class). Maxwell, Warner & Guillen (2021:3) noted that sampling could also be done

systematically, and with different sampling units (e.g. pixels, polygons). Point sampling was chosen because of the different sized outputs from the different classification methods. It was measured against the reference dataset comprised of 213 ground truth samples drawn separately from the training samples:

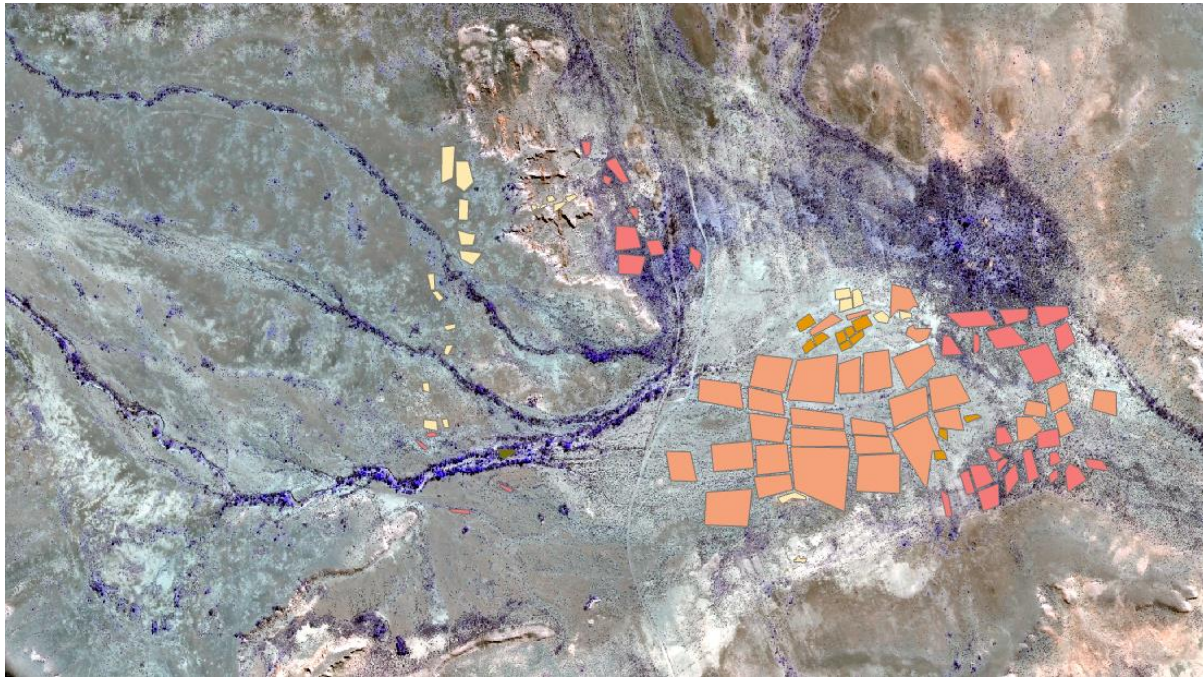


Figure 23-Sample of accuracy reference polygons Scale 1:6613

Table 12- Accuracy Samples for reference dataset

Class	# Samples
Dispersed Chenopod Communities	60
Dense Chenopod Communities	64
Acacia Open Woodlands	15
Bright Sand/Clay	59
Shale Ground	15
Dark Sand	10

A confusion matrix was then computed, together with the metrics used to assess accuracy of the classified result. The confusion matrix lists down in a table format, the classes that were correctly classified and misclassified as other classes. To see the probability that a labelled class is accurate, the user's accuracy is used; to gauge the performance of the classifier for a

particular class, the producer’s accuracy is used. The kappa coefficient is an indicator of overall accuracy that is adjusted for the probability that a positive prediction was made by chance. Formulae of the various metrics of a confusion matrix is as follows:

Measure	Type of Measure	Equation
Overall Accuracy	Integrated Summary	$\frac{\text{Area of map correctly labelled}}{\text{Total area of map}}$
Kappa	Integrated Summary	$\frac{(\text{OA-expected agreement})}{(1-\text{expected agreement})}$
User’s Accuracy (UA)	Class-based	$\frac{\text{Area of map correctly labelled as class x}}{\text{Area of predicted map labelled class x}}$
Producer’s Accuracy (PA)	Class-based	$\frac{\text{Area of map correctly labelled as class x}}{\text{Area of reference map labelled class x}}$

Figure 24- Multiclass metrics derived from a confusion matrix, adapted from (Maxwell, Warner & Guillen 2021: 6)

With the rise of DL methodologies based on CNN in RS classification, (Maxwell, Warner, and Fang 2018: 3) noted that the approaches to measuring accuracy differs slightly from traditional RS accuracy measurements with terminologies like precision, recall, and confidence level.

In some ways, some of the terminologies (precision for user’s accuracy, recall for producer’s accuracy) are interchangeable because of the same way both set of metrics of calculated and for this reason, will be used to compare the performance across the four methods for the classification of the chenopod shrubs.

The Classify objects using deep learning tool, however, only provides precision statistics of its training model, and not for the actual classification results. A manual accuracy assessment check was devised with the following steps:



Figure 25- Manual Accuracy Assessment Tool Check for DL Results

A test set of random points, equalised, and stratified for each class was then generated with the same reference set used previously to produce a confusion matrix in Section 5.4.2.

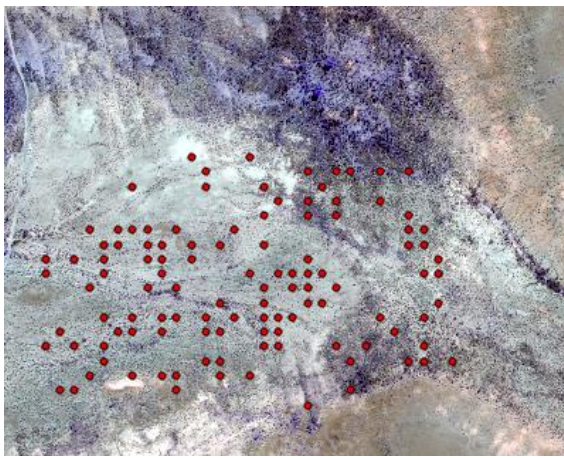


Figure 26- Sample of random accuracy points



Figure 27- 220 Accuracy points distributed across processed DL results

5. RESULTS

The results for the four classification methods are presented below as classified images together with its accuracy results derived from the accuracy reference dataset that was collected with the same process as the training samples.

All results are fully classified images of the study area except for the output from Object Classification using DL due to limitations of the software. However, the tool was run 10 times over the UAV survey areas, a smaller extent compared to the entire study area but nonetheless, provides some representative results of the performance of the DL method. Only the accuracy results from the second attempts of the DL method were retained for comparison with the other three methods.

5.1 Unsupervised Pixel-based Image Classification Results

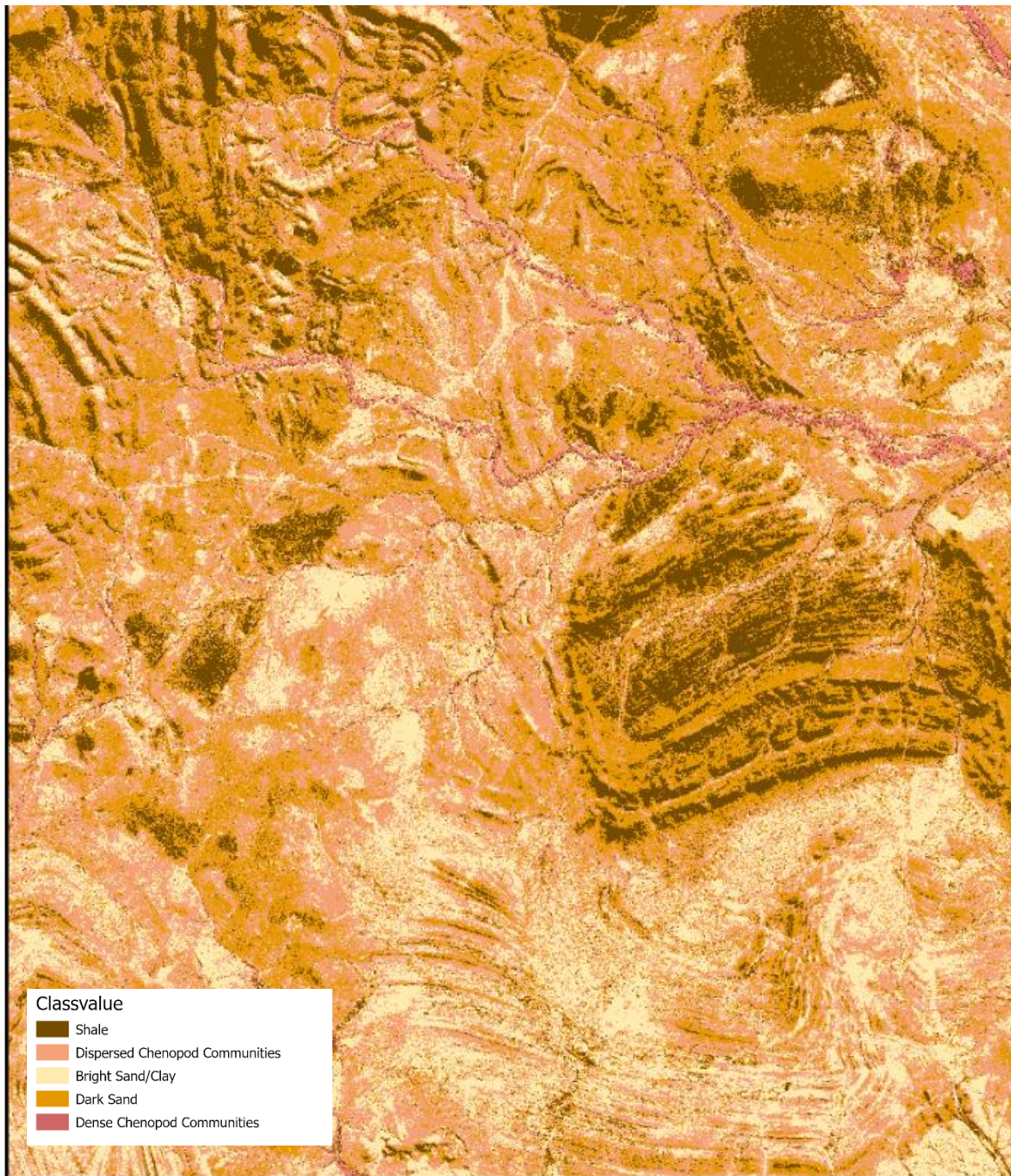


Figure 28- Classified Results from Unsupervised ISO Pixel-based Method

A full map of the classified result is attached as Appendix E, under 9.4.1.

5.1.1 Accuracy Results

Table 13- Confusion Matrix for Unsupervised Classification

ClassValue	C_4	C_3	C_4	C_13	C_12	C_2	Total	U_Accuracy	Kappa
Shale	3	3	0	4	0	15	25	0.12	-
Dispersed Chenopod	0	67	1	0	2	9	79	0.85	-
Bright Sand/Clay	0	41	6	1	5	2	55	0.11	-
Acacia Open Woodlands	0	0	0	0	0	0	0	0	-
Dark Sand	1	25	3	0	6	8	43	0.14	-
Dense Chenopod	0	0	0	15	0	3	18	0.17	-
Total	4	136	10	20	13	37	220	0	-
P_Accuracy	0.75	0.49	0.6	0	0.46	0.08	0	0.39	-
Kappa									0.17

From table 13, the kappa coefficient is low at 0.17, indicating low overall accuracy for classified result. There are no results for Acacia Open Woodlands as the classification only yielded 5 classes instead of 6, as the classifier only managed to detect 5 classes.

5.2 Supervised Pixel Classification Results

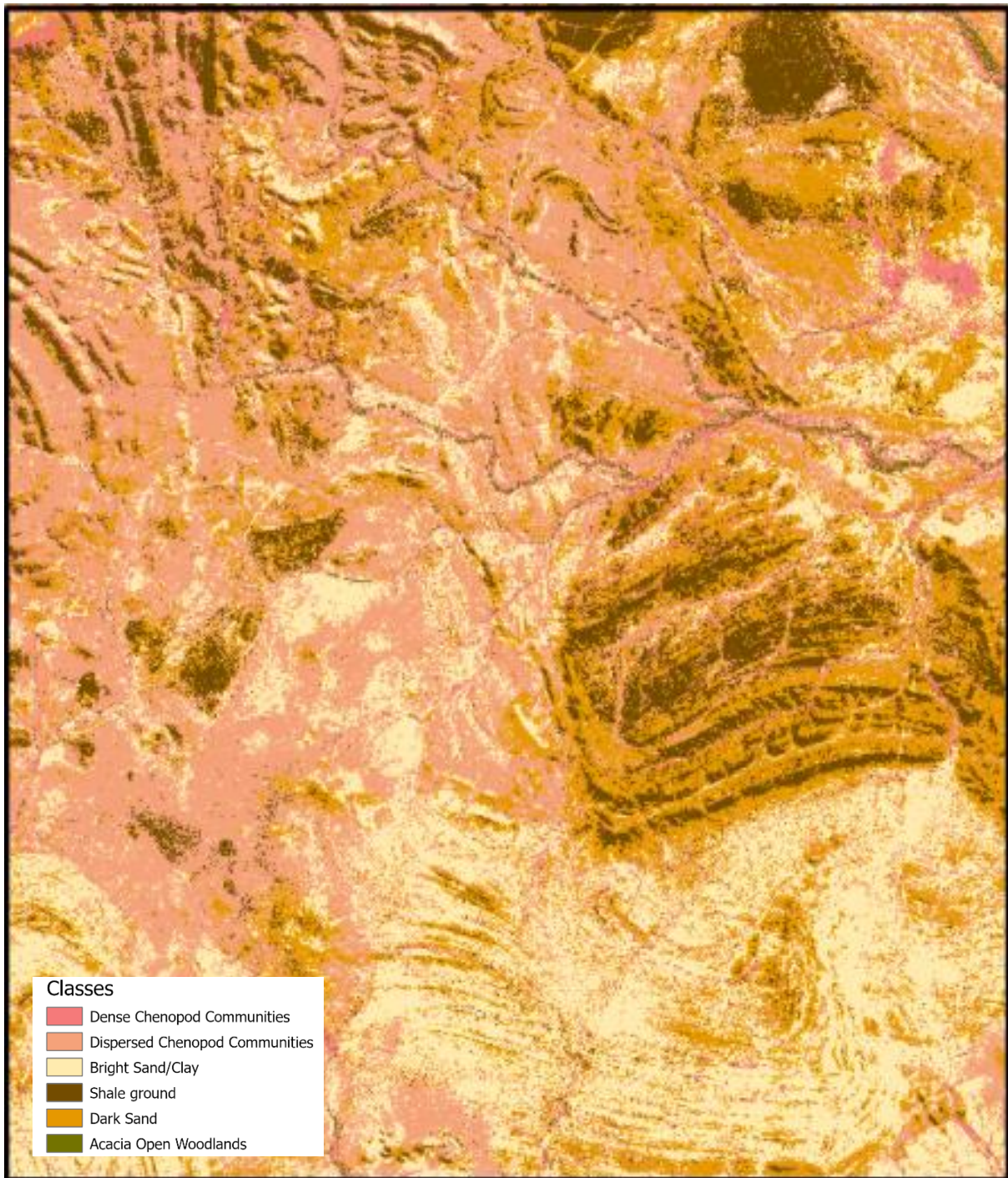


Figure 29-Classified Results from Supervised ML Pixel-based Method

A full map of the classified result is attached as Appendix E, under 9.4.2.

5.2.1 Accuracy Results

Table 14-Confusion Matrix for Supervised Pixel Classification

ClassValue	C_2	C_3	C_4	C_10	C_12	C_13	Total	U_Accuracy	Kappa
Dense Chenopod Communities	305	3	5	2	0	270	585	0.52	-
Dispersed Chenopod Communities	74	272	66	12	0	43	467	0.58	-
Bright Sand/ Clay	41	95	201	0	0	5	342	0.59	-
Shale	32	47	0	451	0	8	538	0.84	-
Dark Sand	41	83	228	35	0	0	387	0	-
Acacia Open Woodlands	7	0	0	0	0	174	181	0.96	-
Total	500	500	500	500	0	500	2500	0	-
P_Accuracy	0.61	0.54	0.40	0.90	0	0.35	0	0.56	-
Kappa									0.47

The kappa coefficient for supervised pixel classification is higher at 0.47 but still considered inaccurate for classification purposes.

5.3 Segmentation Results

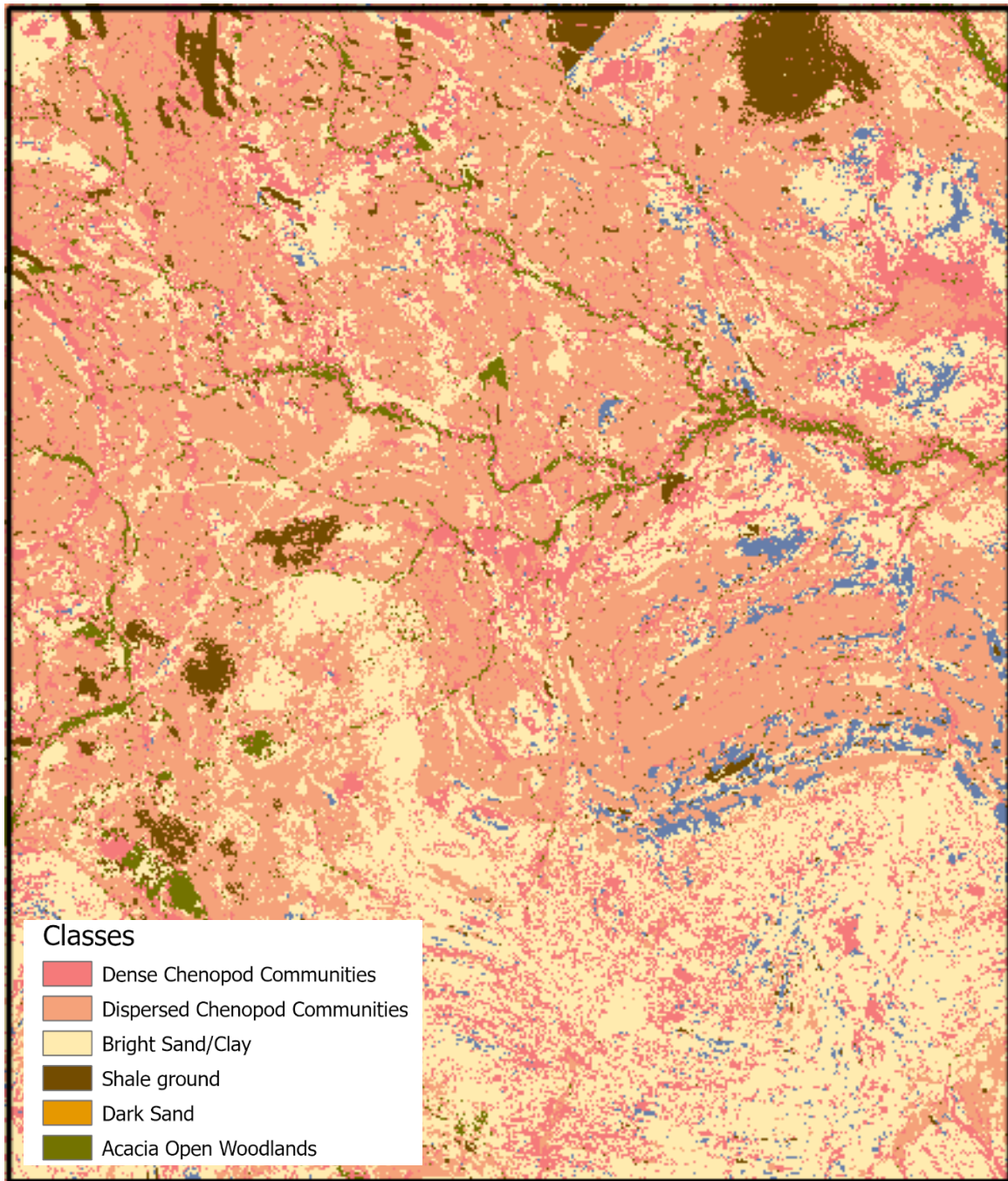


Figure 30- Classified Results from Object-based Segmentation-SVMA full map of the classified result is attached as Appendix E, under 9.4.3.

5.3.1 Accuracy Results

Table 15- Confusion Matrix for Object-based Classification-SVM

ClassValue	C_2	C_3	C_4	C_10	C_13	Total	U_Accuracy	Kappa

Dense Chenopod	398	42	28	0	154	622	0.64	-
Dispersed Chenopod	23	335	150	86	13	607	0.55	-
Bright Sand/Clay	58	90	315	0	45	508	0.62	-
Shale	14	0	0	414	0	428	0.97	-
Acacia Open Woodlands	3	33	0	0	288	324	0.89	-
Total	500	500	500	500	500	2500	0	-
P_Accuracy	0.8	0.67	0.63	0.83	0.58	0	0.7	-
Kappa								0.63

From the table above, it is noted that Dispersed Chenopod Class has the lowest User's accuracy which signifies that a large number of objects were incorrectly classified. It was mostly misclassified as Bright Sand/Clay followed by Shale. Kappa coefficient stands at 0.63 which represents good agreement with ground truth although it stands at the lower end of the strength of agreement.

5.4 Object Classification using Deep Learning

5.4.1 Attempt 1- Classification Results using image_chip size 128 x 128

The Classify Objects using Deep Learning tool was run 8 times at smaller extents because the software was not able to process the classification of the entire image. The areas processed were all survey areas flown by the UAV except for 1e.

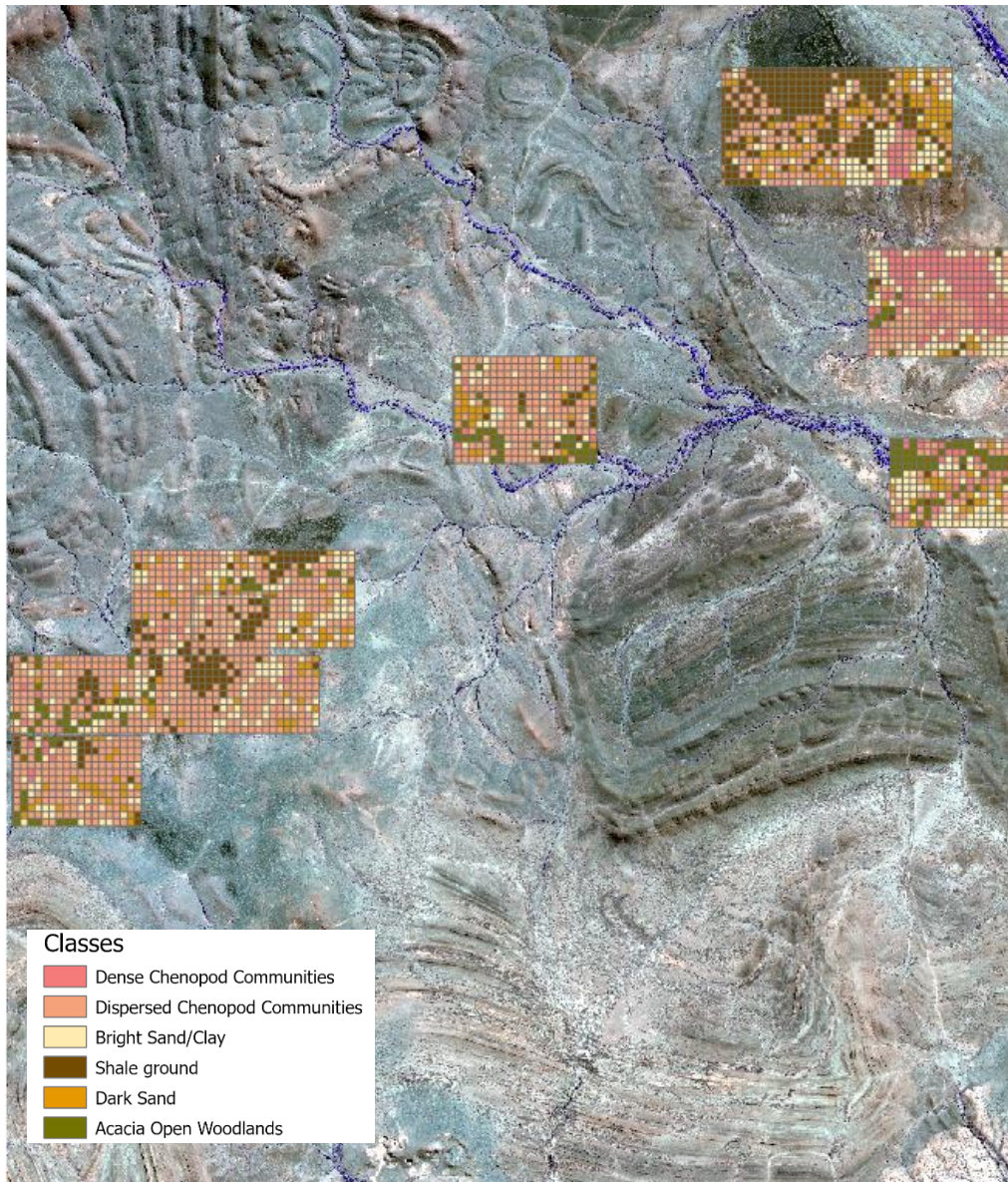


Figure 31- Classified Results from DL- Attempt 1

Model Performance using image chip size 128 x 128

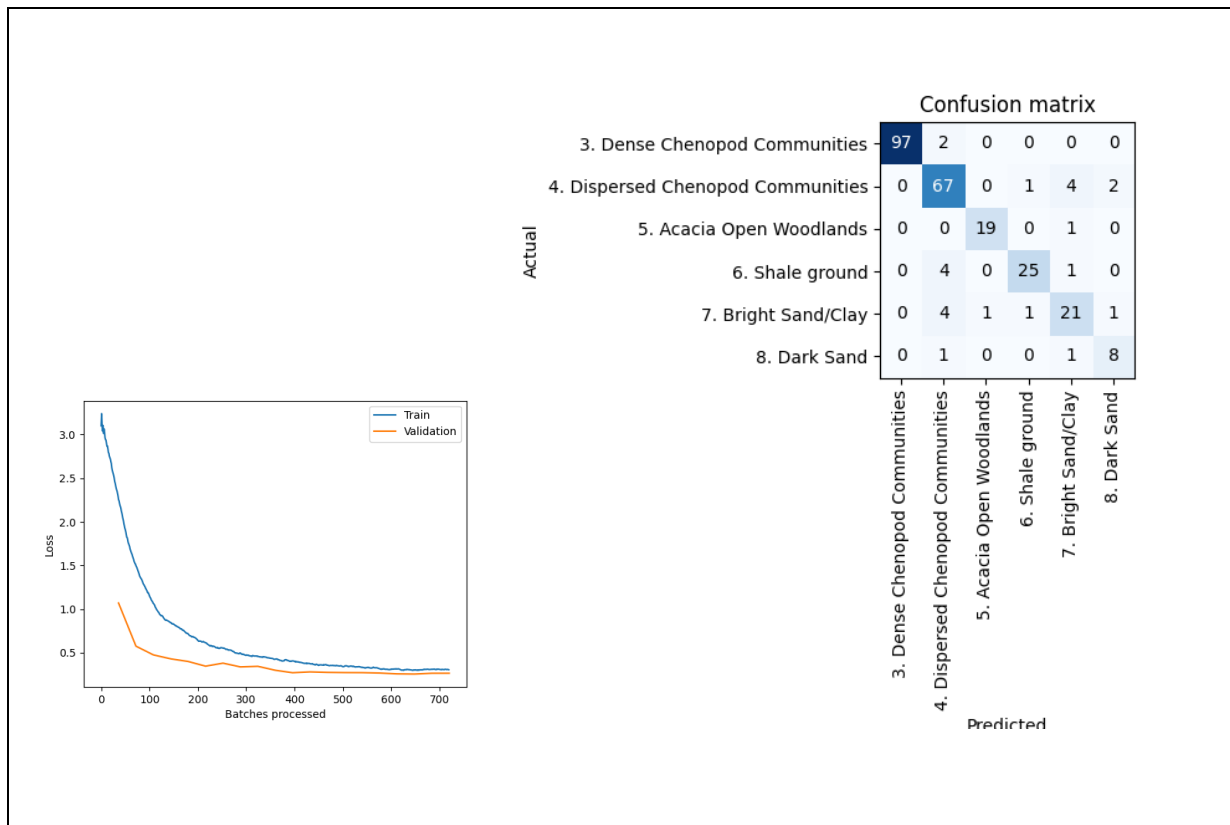


Figure 32-Loss Graph and Confusion Matrix (Attempt 1)

In figure 32 above, we can see that the loss value, representing the errors made for each training set has decreased to a point of stability at the 600 batches mark. A small gap between the training curve and validation curve indicates a good fit and any further training will not yield a better accuracy but might lead to over-fitting of the model instead (Schlüter 2019).

The confusion matrix shows the precision of the deep learning model (not the performance of the classification results itself) by showing the predictions vs the actual classes using the test set (10% of the training set aside during training of the model) as reference.

It shows that for dense chenopod communities, it predicted 97 correctly and misclassified 2 samples as dispersed chenopod communities. For dispersed chenopod communities, it predicted 67 correctly and misclassified 7 as other classes.

Table 16-Confusion Matrix of Training Model of DL Attempt 1- The precision scores and recall scores

Dense Chenopod Shrubs	Dispersed Chenopod Shrubs
-----------------------	---------------------------

TP=97	TN= 162	TP=67	TN= 176
FP= 0	FN= 2	FP= 11	FN= 7
Precision= $97 / (97+0) = 1$ Recall= $97 / (97+2) = \mathbf{0.98}$		Precision= $67 / (67+11) = \mathbf{0.86}$ Recall= $67 / (67+7) = \mathbf{0.71}$	

From table 16, the precision scores and recall scores for dense chenopod communities and dispersed chenopod communities are 1, 0.98 and 0.86, 0.71 respectively.

5.4.2 Attempt 2- Classification Results using image_chip size 64 x 64

Image Classification was run 10 times at smaller extents because the software was not able to process the classification of the entire image. The areas processed were all survey areas flown by the UAV.

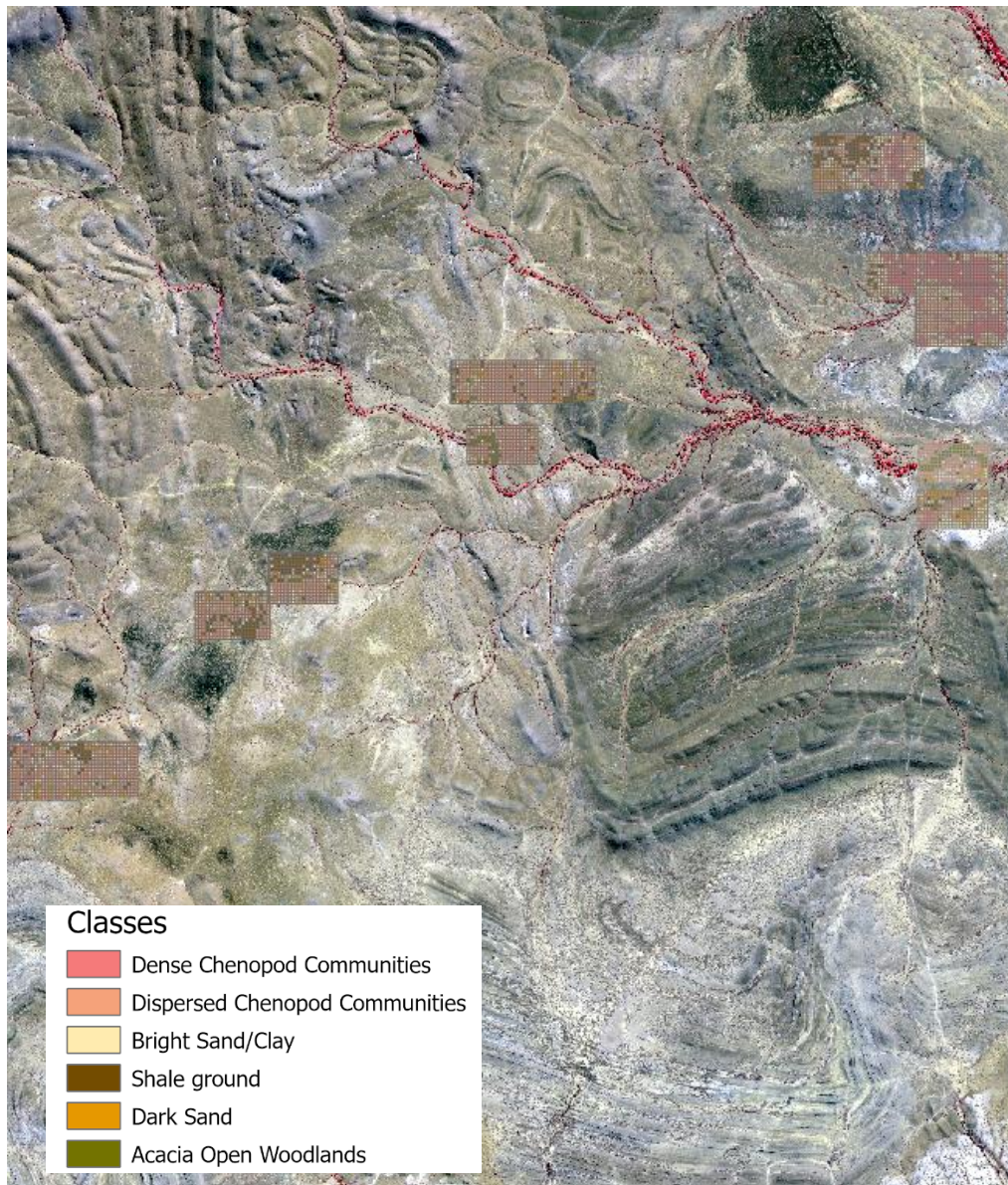


Figure 33- Classified Results from DL- Attempt 2

A full map of the classified result is attached as Appendix E, under 9.4.4.

Model Performance using image chip size 64 x 64

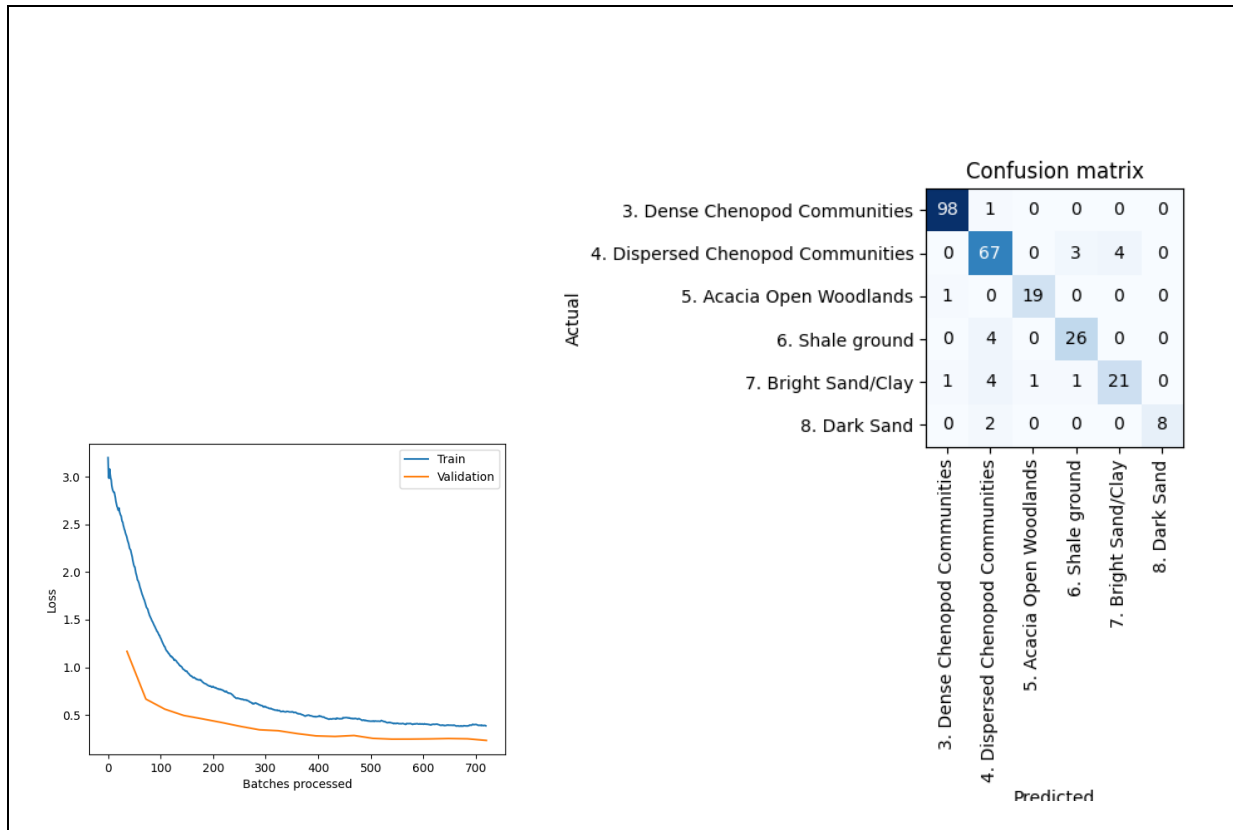


Figure 34- Loss Graph and Confusion Matrix (Attempt 2)

In figure 34 above, we can see that the loss value, representing the errors made for each training set has decreased to a point of stability at the 600 batches mark. A small gap between the training curve and validation curve indicates a good fit and any further training will not yield a better accuracy but might lead to over-fitting of the model instead

It shows that for dense chenopod communities, it predicted 98 correctly and misclassified 1 sample as dispersed chenopod communities. For dispersed chenopod communities, it predicted 67 correctly and misclassified 7 as other classes.

Table 17- Confusion Matrix of Training Model of DL Attempt 1- The precision scores and recall scores

Dense Chenopod Shrubs		Dispersed Chenopod Shrubs	
TP=98	TN= 160	TP=67	TN= 184
FP= 2	FN= 1	FP=11	FN= 7
Precision= $98 / (98+2) = 0.98$		Precision= $67 / (67+11) = 0.86$	

Recall= $98 / (98+1) = 0.99$	Recall= $67 / (67+7) = 0.91$
------------------------------	------------------------------

The precision scores and recall scores for dense chenopod communities and dispersed chenopod communities, from the table above are 0.98, 0.99 and 0.86, 0.91 respectively.

With the performance of both model comparable, further accuracy assessment on the results of the classification output from attempt 2 was done to gauge the actual performance of the classification results.

7.4.1 Accuracy Results

Table 18-Confusion Matrix for Classify Objects using DL (2nd attempt)

ClassValue	Shale	Dispersed Chenopod	Bright Sand/Clay	Acacia Open Woodlands	Dark Sand	Dense Chenopod	Total	U_Accuracy	Kappa
Shale	1	1	1	0	3	1	7	0.14	-
Dispersed Chenopod	1	112	3	1	5	2	124	0.90	-
Bright Sand/Clay	2	5	3	1	3	1	15	0.2	-
Acacia Open Woodlands	0	0	0	16	0	0	16	1	-
Dark Sand	0	1	2	0	2	0	5	0.4	-
Dense Chenopod	0	17	1	2	0	33	53	0.62	-
Total	4	136	10	20	13	37	220	0	-
P_Accuracy	0.25	0.82	0.3	0.8	0.15	0.89	0	0.76	-
Kappa									0.6

5.5 Summary of Accuracy Metrics for the four methods for Chenopod Classes

Table 19- Summary of selected accuracy metrics

Methods/Accuracy Score	User's Accuracy <i>-Dispersed Chenopod Class</i> <i>-Dense Chenopod Class</i>	Producer's Accuracy <i>-Dispersed Chenopod Class</i> <i>-Dense Chenopod Class</i>	Kappa coefficient For all classes
Unsupervised ISO Pixel	0.85 0.17	0.49 0.08	0.17
Supervised Pixel	0.58 0.52	0.54 0.61	0.47
Object-based Segmentation using SVM	0.55 0.64	0.67 0.80	0.63
Object-based Classification using 64*64 chip size	0.90 0.62	0.82 0.89	0.6

5.6 Visual Comparison of Results for two selected areas- Area 2a, 1f

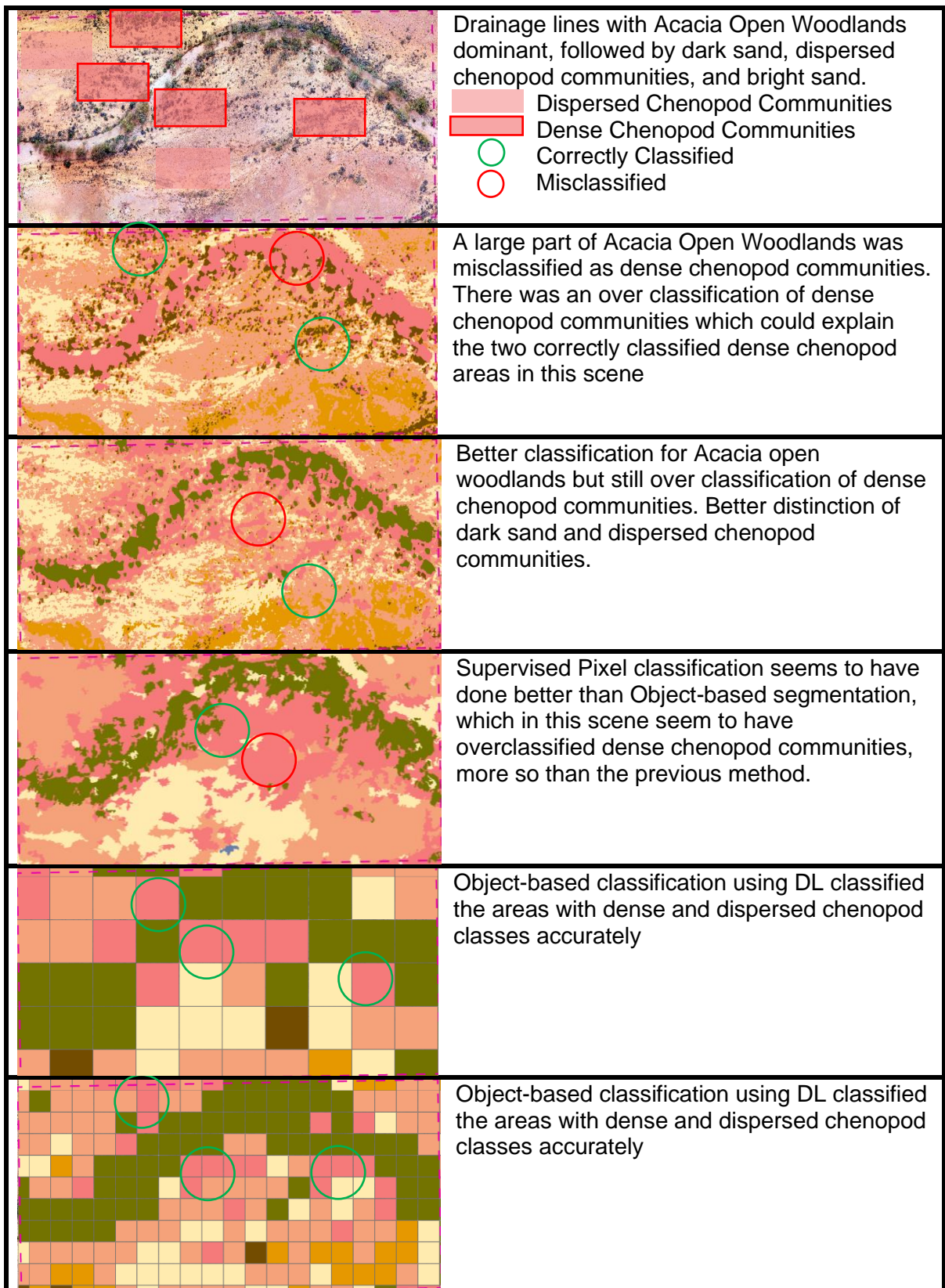


Figure 35- Area 2a- Scale 1:1,1849 In order of results: Orthoimage (ground truth), Unsupervised ISO Pixel Classification, Supervised Pixel Classification, Object-based Classification using SVM, Object-based classification using DL (128*128), Object-based classification using DL (64*64)

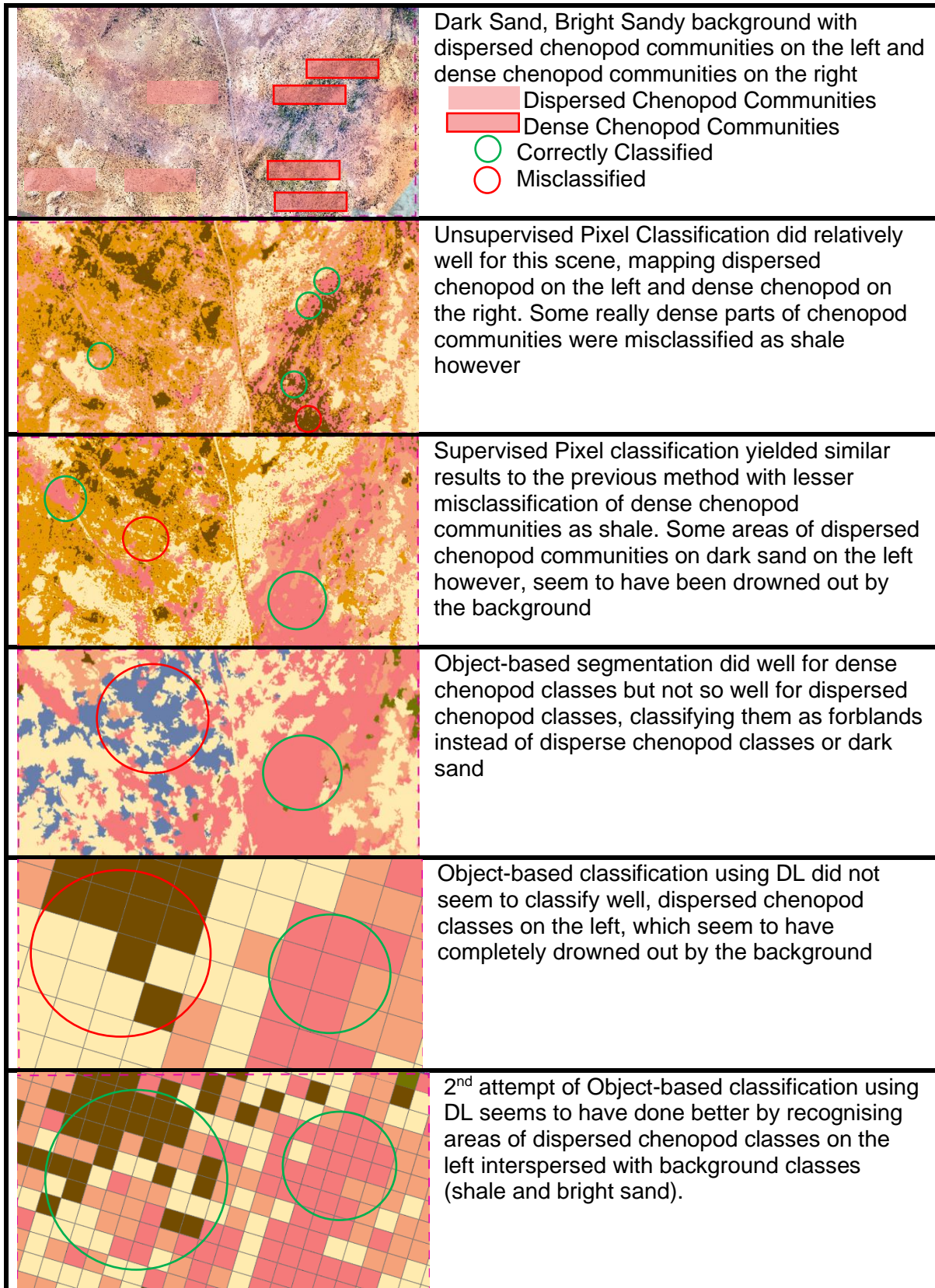


Figure 36- Area 1F- Scale 1:1,1849 In order of results: Orthoimagery (ground truth), Unsupervised ISO Pixel Classification, Supervised Pixel Classification, Object-based Classification using SVM, Object-based classification using DL (128*128), Object-based classification using DL (64*64)

6. DISCUSSION

6.1 Overall Results

The classification results from the four methods have shown varying results in terms of classified results and level of accuracy. Each method is theoretically, mathematically, and procedurally more sophisticated than the method preceding them, and this translates to the accuracy of the thematic map generated when looking at the increasing kappa coefficient figure from the unsupervised pixel-based classification to the object-based classification using DL (see Table 19). According to Table 19, the two most accurate methods are Object-based methods with a kappa coefficient of 0.63 and 0.6 for segmentation and DL respectively. This agrees with the literature, with some authors also noting higher overall accuracy from DL methods (Yue et al. 2015; Huang et al. 2018).

Looking into the metric which measures the percentage of area correctly labelled as dispersed chenopod communities vs all areas labelled as dispersed chenopod communities, the user's accuracy for dispersed chenopod communities is highest for object-based classification using DL (0.9), followed by unsupervised pixel classification (0.85), and then Supervised Pixel Classification (0.58).

While the user's accuracy for the dispersed chenopod shrub class is high for unsupervised pixel classification, the low kappa coefficient for the unsupervised method casts doubts on the accuracy of the figure. It may be highly skewed due to the over classification of areas as dispersed chenopod communities⁵. This is supported by the lower producer's accuracy (0.49) for the same class which denotes the areas correctly labelled as dispersed chenopod communities vs the areas that are actual chenopod communities.

Looking at the metric for dense chenopod class, the highest user's accuracy comes from object-based classification using segmentation (0.64), followed by object-based classification using DL (0.62), and then supervised pixel classification (0.52). The high user's accuracy

⁵ Dispersed Chenopod Communities is the most classified area of the entire results

figure is supported by high producer's accuracy figures (0.8 for segmentation and 0.89 for DL). This means that the percentage of correctly labelled areas vs all areas labelled dense chenopod is fairly high, while the percentage of areas that are correctly labelled as dense chenopod vs areas that are actually dense chenopod is even higher.

Overall, it appears that object-based classification methods do better than pixel-based classification methods for classifying our object of interest under the two main classes, dense and dispersed chenopod communities with both object-based segmentation and DL having comparable accuracies with the latter slightly more accurate than the former. This agrees with the general literature which non-parametric classifiers (as in the object-based methods) have been proven to provide better classification results when classifying complex landscapes (Lu and Weng 2018: 836). Lu and Weng noted that parametric classifiers like ML (which was used in Supervised Pixel-based classification) does not tend to work well on complex landscapes and will generally produce "noisy" results (2018: 830).

When taking other non-chenopod classes (2 ground classes and 1 other vegetation class) into consideration however, object-based segmentation has, on average, a higher user's accuracy than the DL method. This shows that object-based segmentation, which starts from a pixel-based approach may be more suitable for classifying ground classes which tend to have more 'pure' pixels than other object classes.

Further discussions on the results from each method is presented below.

6.2 Limitations of Pixel-based Classification

The results from running pixel-based classification of a small study area in WNR has shown that it does not work as well as the object-based methods for mapping our object of interest, chenopod shrub communities. This can be attributed to a few reasons:

The size of the object of interest is larger than a pixel (0.5m) and has mixed spectral qualities due to a mix of bare ground and vegetation within the object itself. This is especially the case for dispersed chenopod class, where background effect can make up at least half of the object.

This likely led to the common misclassification between dispersed chenopod class and bright sand/clay class- as seen from table 13, and table 14 where 41 out of 55 bright sand/clay pixels were misclassified as dispersed chenopod, and 95 out of 342 pixels classified by supervised pixel classification were misclassified as dispersed chenopod.

Pixel-based classification methods which assigns a class pixel by pixel only according to its spectral qualities would not be able to assign accurately a class with mixed spectral reflectance value to pixels with pure reflectance value (Fisher 1997, Cracknell 1998 cited in Lu and Weng 2007: 836).

Supervised ML pixel classification, however, appears to produce better results compared to unsupervised ISO pixel classification. This can be seen from the consistent higher user's and producer's accuracies for both Dispersed and Dense chenopod classes. This could be due to the sufficient training samples (a total of 763 sample) provided to the software as a parametric classifier like ML is likelier to yield an accurate result with more samples available (Lu & Weng 2007:839).

The User's Accuracy for Supervised classification for Dense Chenopod Communities and Dispersed Chenopod Communities was 0.52 and 0.58 respectively, relatively lower than the accuracy results for other non-chenopod classes which ranged from 0.58-0.96.

Dense chenopod communities were often misclassified as Acacia Open Woodlands, while Dispersed chenopod communities were often misclassified as Bright Sand/Clay due to the preponderance of Bright Sand/Clay in Dispersed Chenopod Communities. These two classes were often misclassified as each other due to its characteristics and would prove to be the difficult class to classify across all four methods. Pixel classification, however, did relatively well for Acacia Open Woodlands and Shale with User's accuracy at 0.96 and 0.84 respectively. This can be attributed to the distinct spectral reflectance for both classes compared to other classes and it appears that pixel-based classification does well for classes with distinct spectral reflectance due to its focus on spectral quality when classifying.

6.3 Limitations of Object-based segmentation classification

Accuracy rates for dense chenopod class is generally acceptable at 0.64, however, dispersed chenopod class has a lower accuracy rate at 0.55 with misclassification of dispersed chenopod classes prevalent, as in the case with other methods.

Given the minimum pixel size of each segment (80 pixels), individual adult chenopod shrubs were not classified, with only chenopod communities at a minimum of 80 pixels (m wide approximately) being mapped.

While kappa coefficient for Object-based segmentation is higher than pixel-based methods at 0.63, its user's accuracy for dispersed chenopod class did not differ too much from the supervised pixel classification method, in fact, it is 0.03 lower than the latter. While it does considerably better than supervised pixel for dense chenopod classes, its performance for dispersed chenopod is comparable with supervised pixel classification.

6.4 Limitations of Deep Learning- CNN

(Wu et al. 2021: 3) noted a large amount of training samples, with even distribution across the study area is needed for representative sampling to achieve high accuracy rates for deep learning classification. However, he also noted that with many studies now using pre-trained classifiers with transfer learning, those limitations could be plugged.

Object classification using DL while producing excellent results for dispersed chenopod class (according to the matrix and visuals in table 18 and figure 36), did no better than object-based SVM for dense chenopod class. Dense chenopod areas were most often misclassified as dispersed chenopod classes with 17 out of 53 (32%) misclassified as dispersed chenopod classes for example (table 18). Given similar contextual information and characteristics between the two classes, and similar visuals, it is not surprising that the two tends to be misclassified. Object-based segmentation however, managed to produce a better result, likely because of the spectral signature of dense chenopod class and the way segmentation has managed to group all suitable pixels from that spectral signature as one coherent object which

demonstrates that segmentation has its advantages for object classes that can be defined by its spectral signature. Segmentation, however, will not be as effective for classes that have higher proportion of background or ground pixels in its class, and DL may be better in classifying those as its focuses more on textural information.

Although the literature states that DL approaches tend to outperform classification methods using SVM and other approaches for classification results (Huang et al. 2020: 3473) (Yue et al. 2015), the object of interest in those studies needs to be taken into consideration when citing those high accuracy figures. In Yue et al.'s study for example, while her comparison between DL and SVM methods showed that the former yielded considerably higher overall agreement and kappa coefficient, the object analysed was a hyperspectral image which has pixel values and textural information completely different from an RGB image, which was used in this study.

The accuracy results from DL methods demonstrates the need for separate accuracy assessment to be conducted in addition to the precision figures for model performance, which tends to be overstated.

While DL approach is generally accurate and especially accurate for the dispersed chenopod class (where other methods are found lacking), it also has some specific requirements including the need for many training samples and high computing capabilities in the form of a power GPU processor. Although the classification output is not as fine as the pixel-based methods and object-based segmentation, the resolution of the classified area is adequate for informing land management and conservation strategies.

6.5 Comparison of classification methods

Object-based tools are on the whole, better than Pixel-based tools for classifying Chenopod shrub communities' classes. They work better because chenopod shrub communities are complex objects with varying shapes, and spectral qualities because of the way the shrubs are interspersed into the background. As discussed in the earlier sections, the dispersed chenopod shrub class is the trickiest to classify and tends to be misclassified because of the similar spectral reflectance for sparse chenopod communities with large portion of background. Hence, image context, which is used more in object-based classification methods is more important for classifying these objects, making object-based methods using both segmentation and DL approaches better for classifying landscapes with large proportion of background. Between segmentation and DL, the results have also shown that with the former outperforming the latter for the dense chenopod class, spectral details matter more when classifying certain object.

The varying results across the four classification methods tie in with the literature that classification performance is multi-faceted. There are factors that are more important and according to Khatami, Mountrakis, and Stehman (2016), the inclusion of textural information yields the greatest improvement in accuracy for classification while inclusion of spectral information based in index yield much smaller improvements in accuracy.

When considering the object of interest. Pixel-based classification might be more suitable for homogenous land types with huge swathes of homogenous areas, e.g., bare soil, sand, dense forest which would be likely to produce 'pure' pixels with one unique component. For mapping landscapes, because of the variance in spectral information within a class, object-based classification methods are more suitable than pixel-based methods (Buscombe & Ritchie 2018).

6.6 Potential datasets to augment image-based classification

Apart from solely using imagery (with reflectance value and texture) to classify vegetation, auxiliary environmental data could also have been used to augment the classification process. Examples of these data include altitude, aspect, soil type, and precipitation to aid in the classification of forested areas in Greater Yellowstone Area (Burrough et al. 2001 cited in Wu et al. 2021: 3)

In Wu et al. own study for example, up to 73 environmental variables were extracted and ranked by importance, noting that climate-related factors followed by terrain-related factors influence vegetation classification, with notable factors including elevation and slope in the distribution of vegetation in their study area (2021: 18).

Although our study area is relatively flat in terms of elevation, high-resolution DEM, precipitation data, topographic wetness, and detailed soil-type maps if attainable for this study area can be considered for incorporation into the classification methodology to augment the object-based classification results. These datasets can function as multiple features or explanatory variables linked to the proliferation of chenopod shrubs to produce spatial classifiers for verifying training samples in order to produce more accurate training samples for object classification (Wu et al. 2021: 7).

Apart from auxiliary data, classification results from pixel-based classification could also be used to augment the output from the DL classification by using it to train DL models. Buscombe & Ritchie demonstrated the feasibility of this hybrid method using a conditional random fields (CRFs) modelling for predicting classes for each pixel in an image. The image is then divided into training tiles with fixed sample tile size and exported as training tiles with its label being the class label with the highest proportion of pixels classified as that class. This has proven to achieve higher levels of accuracies for DL landscape-classification at a finer level compared to conventional DL frameworks (Buscombe and Ritchie 2018: 17) Conventional DL frameworks often lose spatial resolution when pooling and may cause label images to appear “coarse” at object/label boundaries. Conventional DL frameworks also

typically need larger, more sophisticated DL architecture, (not to mention more training samples) in order to produce a similarly accurate classification at a finer scale. With the hybrid method, the authors have developed a way to incorporate pixel-classification into DL to produce better accuracy at finer-scale if needed⁶. This shows that pixel-based methods, although generally with lower accuracies when classifying landscapes, can complement DL methods with advanced methods of data processing.

⁶ Another study used a similar hybrid method (with CRFs) to map weeds in rice crops and found that the hybrid method also produced better accuracy, 13.6% higher than OBIA (Huang et al. 2018)

7. CONCLUSION

As noted earlier at the start of this study, the wide array of remote sensing applications means that there is no one standard process nor universal criterion for data imagery or processing steps (Sandino et al. 2018: 2).

This study has demonstrated the potential of using a wide array of classification methods with a corresponding algorithm, and attempted to make a straightforward comparison between the performance of each classification methods for mapping the habitat of the TBGW for conservation purposes and the benefits and drawbacks of each method.

While it has demonstrated better performance from object-based and DL methods for mapping our object of interest, further studies can be done to examine how to improve the accuracy rates for our object of interest given that classification of the natural environment are inherently difficult due to the complex composition of the image, unlike in an urban setting where objects to be classified tend to be spectrally and spatially homogenous, with distinct and sharp edges.

Further studies could also compare the performance of certain algorithms and DL architectures. This study, which compared the performance of 4 classification methods, did not have the scope to compare algorithm performance with the use of a control method, for example object-based segmentation with ML vs SVM or DL model training with a different architecture.

While DL methods have been proven in this study to produce good accuracy results for classification of complex scenes, it remains to be seen if there will be higher uptake of DL approaches for classification tasks. In a meta-analysis of 1651 articles, Yu et al. (2014) found that 32% of the articles employed parametric methods using ML classifiers, with non-parametric SVM segmentation methods coming in a close second. This was attributed to the wide availability of software tools that uses these methods. Given the difficulty and added steps needed for DL approaches to classification tasks, it is unclear if DL approaches will gain currency as an accurate and reliable method for mapping vegetation like the chenopod shrubs.

Maxwell, Warner, and Fang and Richards et al. (2018: 2785; 2013: 381) opined that once RS users are more familiar with the processes and concepts of DL, it is predicted that more studies will be employing DL methods for satellite imagery classification.

At the moment, the study shows a potential for DL approaches for mapping chenopod shrubs in a complex environment across the entire WNR. It demonstrates the primary steps and pre-processing needed in order to achieve a relatively accurate mapping of the habitat of the TBGW. A classified map at the resolution produced in Attempt 2 of the DL classification provides enough spatial information on chenopod shrubs country for land managers to focus conservation efforts in specific areas given limited resources and time, in order to achieve efficiencies in conservation efforts. Traditional in-situ vegetation surveys will never be able to scale-up to the level of RS in trying to map entire nature reserve with similar levels of resources and manpower. Combining the results from this classification process with the observations of the TBGW in the future can help develop further insights into the effectiveness of conservation activities on a spatial level.

8. REFERENCES

- Al-Ali, Z. M., M. M. Abdullah, N. B. Asadalla, and M. Gholoum. 2020. 'A comparative study of remote sensing classification methods for monitoring and assessing desert vegetation using a UAV-based multispectral sensor', *Environ Monit Assess*, 192: 389.
- Al-Bukhari, Abdulsalam, Stephen Hallett, and Tim Brewer. 2018. 'A review of potential methods for monitoring rangeland degradation in libya', *Pastoralism : research, policy and practice*, 8: 1-14.
- Alshari, Eman A., and Bharti W. Gawali. 2021. 'Development of classification system for LULC using remote sensing and GIS', *Global Transitions Proceedings*, 2: 8-17.
- Bhatnagar, Saheba, Laurence Gill, and Bidisha Ghosh. 2020. 'Drone Image Segmentation Using Machine and Deep Learning for Mapping Raised Bog Vegetation Communities', *Remote Sensing*, 12.
- Blaschke, Thomas, Stefan Lang, and Geoffrey Hay. 2008. *Object-Based Image Analysis Spatial Concepts for Knowledge-Driven Remote Sensing Applications* (Berlin, Heidelberg : Springer Berlin Heidelberg : Imprint: Springer).
- Burnham, Colin. 2019. "A Study of UAV Photogrammetry Software." In *Research Gate*.
- Buscombe, Daniel, and Andrew C. Ritchie. 2018. 'Landscape classification with deep neural networks', *Geosciences (Basel)*, 8: 244.
- Cai, Dingding, Ke Chen, Yanlin Qian, and Joni-Kristian Kämäräinen. 2019. 'Convolutional low-resolution fine-grained classification', *Pattern Recognition Letters*, 119: 166-71.
- Campbell, James B. 2011. *Introduction to Remote Sensing, Fifth Edition* (New York: Guilford Publications).
- Chen, Gang, Qihao Weng, Geoffrey J. Hay, and Yinan He. 2018. 'Geographic object-based image analysis (GEOBIA): emerging trends and future opportunities', *GIScience and remote sensing*, 55: 159-82.
- Courtial, Azelle, Achraf El Ayedi, Guillaume Touya, and Xiang Zhang. 2020. 'Exploring the potential of deep learning segmentation for mountain roads generalisation', *ISPRS international journal of geo-information*, 9: 338.
- Dash, Jonathan P., Grant D. Pearse, and Michael S. Watt. 2018. 'UAV multispectral imagery can complement satellite data for monitoring forest health', *Remote sensing (Basel, Switzerland)*, 10: 1216.
- del Río-Mena, Trinidad, Louise Willemen, Ghirmay Tsegay Tesfamariam, Otto Beukes, and Andy Nelson. 2020. 'Remote sensing for mapping ecosystem services to support evaluation of ecological restoration interventions in an arid landscape', *Ecological indicators*, 113: 106182.
- Department for Environment and Heritage. 2009. "Stony Plains Conservation Priorities." In *South Australian Arid Lands Biodiversity Strategy*, edited by South Australian Arid Lands NRM Board.
- Department of Agriculture Water and the Environment. 2020. 'National Vegetation Information System (NVIS)'. https://www.environment.gov.au/land/native-vegetation/national-vegetation-information-system#NVIS_data_products.
- . 2021. 'Witchelina', Accessed 24 March 2021. <https://www.environment.gov.au/land/nrs/case-studies/sa/witchelina>.
- . 2021. 'National Vegetation Information System Taxonomic Review', Accessed 10 September 2021. <https://www.awe.gov.au/agriculture-land/land/publications/nvis-taxonomic-review/introduction>
- Department of Water, Land, and Biodiversity Conservation. 2009. Witchelina Station Map.
- Department of Environment, Water, and the Government of South Australia Natural Resources. 2020. 'Our Region', Accessed 2 March 2021. <https://www.landscape.sa.gov.au/saal/about-us/our-region>.

- ESRI. 2021a. 'Train ISO Cluster Classifier (Image Analyst)', Accessed 10 August. <https://pro.arcgis.com/en/pro-app/latest/tool-reference/image-analyst/train-iso-cluster-classifier.htm>.
- . 2021b. 'Train Maximum Likelihood Classifier (Image Analyst)', Accessed 10 August. <https://pro.arcgis.com/en/pro-app/latest/tool-reference/image-analyst/train-maximum-likelihood-classifier.htm>.
- . 2021c. 'Train Support Vector Machine Classifier (Image Analyst)', Accessed 10 August. <https://pro.arcgis.com/en/pro-app/latest/tool-reference/image-analyst/train-support-vector-machine-classifier.htm>.
- . 2021d. 'Understanding segmentation and classification', Accessed 2 October. <https://pro.arcgis.com/en/pro-app/latest/tool-reference/image-analyst/understanding-segmentation-and-classification.htm>.
- ESRI Inc. 2020. "ArcGIS Pro." Version 2.80.
- Fisk, Claire, Kenneth D Clarke, and Megan M Lewis. 2019. 'Comparison of hyperspectral versus traditional field measurements of fractional ground cover in the Australian arid zone', *Remote Sensing*, 11: 2825.
- Glenn, Edward P., Alfredo R. Huete, Pamela L. Nagler, and Stephen G. Nelson. 2008. 'Relationship Between Remotely-sensed Vegetation Indices, Canopy Attributes and Plant Physiological Processes: What Vegetation Indices Can and Cannot Tell Us About the Landscape', *Sensors (Basel)*, 8: 2136-60.
- Gray, Patrick C., Justin T. Ridge, Sarah K. Poulin, Alexander C. Seymour, Amanda M. Schwantes, Jennifer J. Swenson, and David W. Johnston. 2018. 'Integrating drone imagery into high resolution satellite remote sensing assessments of estuarine environments', *Remote sensing (Basel, Switzerland)*, 10: 1257.
- He, K., Zhang, X., Ren, S. and Sun, J., 2016. Deep residual learning for image recognition. In *Proceedings of the IEEE conference on computer vision and pattern recognition* (pp. 770-778).
- Hossain, Mohammad D., and Dongmei Chen. 2019. 'Segmentation for Object-Based Image Analysis (OBIA): A review of algorithms and challenges from remote sensing perspective', *ISPRS Journal of Photogrammetry and Remote Sensing*, 150: 115-34.
- Hu, Fan, Gui-Song Xia, Jingwen Hu, and Liangpei Zhang. 2015. 'Transferring deep convolutional neural networks for the scene classification of high-resolution remote sensing imagery', *Remote sensing (Basel, Switzerland)*, 7: 14680-707.
- Huang, Huasheng, Jizhong Deng, Yubin Lan, Aqing Yang, Xiaoling Deng, and Lei Zhang. 2018. 'A fully convolutional network for weed mapping of unmanned aerial vehicle (UAV) imagery', *PLoS One*, 13: e0196302-e02.
- Huang, Huasheng, Yubin Lan, Aqing Yang, Yali Zhang, Sheng Wen, and Jizhong Deng. 2020. 'Deep learning versus Object-based Image Analysis (OBIA) in weed mapping of UAV imagery', *International Journal of Remote Sensing*, 41: 3446-79.
- Huete, Alfredo, Kamel Didan, Tomoaki Miura, E Patricia Rodriguez, Xiang Gao, and Laerte G Ferreira. 2002. 'Overview of the radiometric and biophysical performance of the MODIS vegetation indices', *Remote sensing of environment*, 83: 195-213.
- Iizuka, Kotaro, Masayuki Itoh, Satomi Shiodera, Takashi Matsubara, Mark Dohar, and Kazuo Watanabe. 2018. 'Advantages of unmanned aerial vehicle (UAV) photogrammetry for landscape analysis compared with satellite data: A case study of postmining sites in Indonesia', *Cogent geoscience*, 4: 1498180.
- Jafari, Reza. 2007. 'Arid land condition assessment and monitoring using multispectral and hyperspectral imagery'.
- Jones, Eriita G., Sebastien Wong, Anthony Milton, Joseph Sclauzero, Holly Whittenbury, and Mark D. McDonnell. 2020. 'The Impact of Pan-Sharpener and Spectral Resolution on Vineyard Segmentation through Machine Learning', *Remote Sensing*, 12: 934.
- Khatami, Reza, Giorgos Mountrakis, and Stephen V. Stehman. 2016. 'A meta-analysis of remote sensing research on supervised pixel-based land-cover image classification processes: General guidelines for practitioners and future research', *Remote sensing of environment*, 177: 89-100.

- Kumar, Anil, Priyadarshi Upadhyay, and A. Senthil Kumar. 2020. *Fuzzy Machine Learning Algorithms for Remote Sensing Image Classification* (Taylor & Francis Group: Milton, UNITED KINGDOM).
- Laben, Craig A, and Bernard V Brower. 2000. "Process for enhancing the spatial resolution of multispectral imagery using pan-sharpening." In.: Google Patents.
- Li, Miao, Shuying Zang, Bing Zhang, Shanshan Li, and Changshan Wu. 2014. 'A Review of Remote Sensing Image Classification Techniques: the Role of Spatio-contextual Information', *European journal of remote sensing*, 47: 389-411.
- Lindenmayer, David, Emma Burns, Nicole Thurgate, and Andrew Lowe. 2014. "The value of long-term research and how to design effective ecological research and monitoring." In *Biodiversity and environmental change : monitoring, challenges and direction*, edited by David Lindenmayer. Melbourne: Collingwood : CSIRO Publishing.
- Louter, M. 2016. The behavioural ecology of the thick-billed grasswren. Flinders University, School of Biological Sciences.
- Lu, D., and Q. Weng. 2007. 'A survey of image classification methods and techniques for improving classification performance', *International Journal of Remote Sensing*, 28: 823-70.
- Malatesta, Luca, Fabio Attorre, Alfredo Altobelli, Ahmed Adeeb, Michele De Sanctis, Nadim M Taleb, Paul T Scholte, and Marcello Vitale. 2013. 'Vegetation mapping from high-resolution satellite images in the heterogeneous arid environments of Socotra Island (Yemen)', *Journal of Applied Remote Sensing*, 7: 073527.
- Marshall, V. M., M. M. Lewis, and B. Ostendorf. 2014. 'Detecting new Buffel grass infestations in Australian arid lands: evaluation of methods using high-resolution multispectral imagery and aerial photography', *Environ Monit Assess*, 186: 1689-703.
- Maxwell, Aaron E., Timothy A. Warner, and Fang Fang. 2018. 'Implementation of machine-learning classification in remote sensing: an applied review', *International Journal of Remote Sensing*, 39: 2784-817.
- Meyer, T., and G. S. Okin. 2015. 'Evaluation of spectral unmixing techniques using MODIS in a structurally complex savanna environment for retrieval of green vegetation, nonphotosynthetic vegetation, and soil fractional cover', *Remote sensing of environment*, 161: 122-30.
- Meyera, P., K. Staenzb, and K. I. Ittena. 1996. 'Semi-automated procedures for tree species identification in high spatial resolution data from digitized colour infrared-aerial photography', *ISPRS Journal of Photogrammetry and Remote Sensing*, 51: 5-16.
- Nagendra, Harini, Richard Lucas, João Pradinho Honrado, Rob H. G. Jongman, Cristina Tarantino, Maria Adamo, and Paola Mairota. 2013. 'Remote sensing for conservation monitoring: Assessing protected areas, habitat extent, habitat condition, species diversity, and threats', *Ecological indicators*, 33: 45-59.
- Namyatova, Anna A, Michael Elias, and Gerasimos Cassis. 2011. 'A new genus and two new species of Orthotylinae (Hemiptera: Heteroptera: Miridae) from central Australia', *Zootaxa*, 2927: 38-48.
- Namyatova, Anna A, Michael D Schwartz, and Gerasimos Cassis. 2013. 'First record of the genus *Stenotus* Jakovlev from Australia, with two new species, and a list of mirine species from Witchelina Nature Reserve (Insecta: Heteroptera: Miridae: Mirinae: Mirini)', *Journal of Natural History*, 47: 987-1008.
- Natural Resource South Australia. 2017. "Native Vegetation Council Rangelands Assessment Manual." In, edited by Native Vegetation Branch.
- Ni-Bin, Chang. 2011. 'Structured Systems Analysis for Sustainable Design.' in (McGraw-Hill Education: New York).
- NVIS Technical Working Group. 2017. "Australian Vegetation Attribute Manual: National Vegetation Information System, Version 7.0." In, edited by Department of the Environment and Energy. Canberra, Australia.

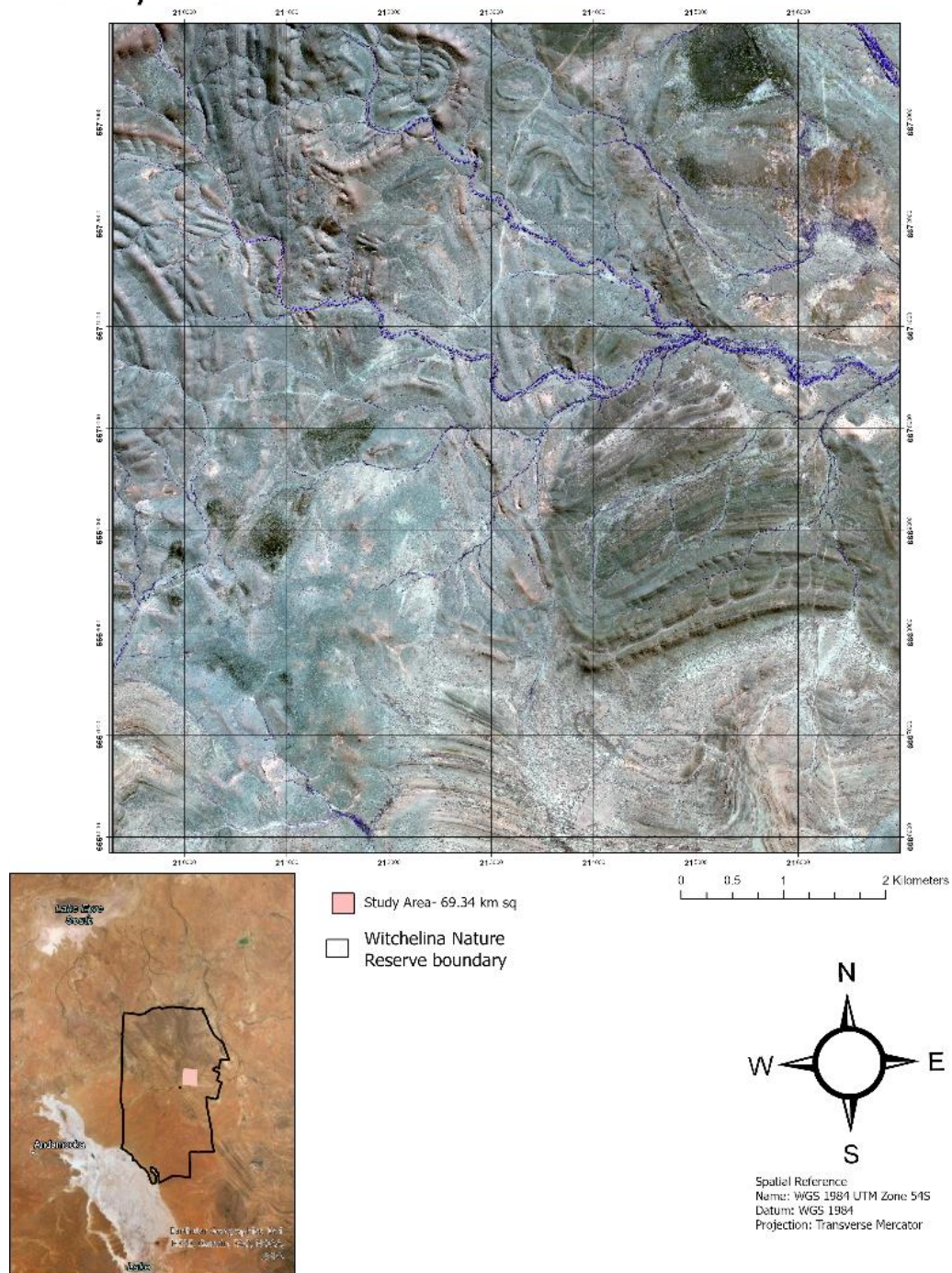
- Okin, Gregory S. , and Dar A. Roberts. 2004. 'Manual of Remote Sensing.' in Susan L Ustin (ed.), *Remote Sensing in Arid Regions: Challenges and Limitations* (John Wiley & Sons).
- Olsson, Aaryn D., Willem J. D. van Leeuwen, and Stuart E. Marsh. 2011. 'Feasibility of invasive grass detection in a desertscrub community using hyperspectral field measurements and landsat TM imagery', *Remote sensing (Basel, Switzerland)*, 3: 2283-304.
- Phinn, S., J. Franklin, A. Hope, D. Stow, and L Huenneke. 1996. 'Biomass Distribution Mapping Using Airborne Digital Video Imagery and Spatial Statistics in a Semi-Arid Environment', *Journal of Environmental Management*, 47: 139-64.
- pix4D. 2021a. 'Image acquisition', Accessed 2 August 2021. <https://support.pix4d.com/hc/en-us/articles/115002471546-Image-acquisition>.
- . 2021b. 'Processing Options- Initial Processing- Matching'. <https://support.pix4d.com/hc/en-us/articles/205433155-Menu-Process-Processing-Options-1-Initial-Processing-Matching#label2>.
- Poon, Joanne. 2007. *Spatial information generation from high-resolution satellite imagery* (University of Melbourne, Department of Geomatics).
- Qi, Jianguo, Abdelghani Chehbouni, Alfredo R Huete, Yann H Kerr, and Soroosh Sorooshian. 1994. 'A modified soil adjusted vegetation index', *Remote sensing of environment*, 48: 119-26.
- Richards, John A. 2013. 'Sources and Characteristics of Remote Sensing Image Data.' in, *Remote Sensing Digital Image Analysis: An Introduction* (Springer Berlin Heidelberg: Berlin, Heidelberg).
- Sandino, Juan, Felipe Gonzalez, Kerrie Mengersen, and Kevin Gaston. 2018. 'UAVs and Machine Learning Revolutionising Invasive Grass and Vegetation Surveys in Remote Arid Lands', *Sensors*, 18: 605.
- Sankey, Temuulen T., Jason McVay, Tyson L. Swetnam, Mitchel P. McClaran, Philip Heilman, Mary Nichols, Nathalie Pettorelli, and Ned Horning. 2018. 'UAV hyperspectral and lidar data and their fusion for arid and semi-arid land vegetation monitoring', *Remote sensing in ecology and conservation*, 4: 20-33.
- Schlüter, Nils. 2019. "Don't Overfit! — How to prevent Overfitting in your Deep Learning Models." In *Towards Data Science*.
- Slender, Amy L, Marina Louter, Michael G Gardner, and Sonia Kleindorfer. 2018. 'Thick-billed grasswren (*Amytornis modestus*) songs differ across subspecies and elicit different subspecific behavioural responses', *Transactions of the Royal Society of South Australia*, 142: 105-21.
- TERN. 2021. 'About Page', Accessed 10 July. <https://www.tern.org.au/tern-observatory/tern-landscapes/>.
- Trimble Inc. 2021. 'What is eCognition?', Accessed 10 September 2021. <https://geospatial.trimble.com/what-is-ecognition>
- Ustin, Susan L., and John A. Gamon. 2010. 'Remote sensing of plant functional types', *New Phytol*, 186: 795-816.
- Vaidya, Bhaumik, and Chirag Paunwala. 2019. 'Deep Learning Architectures for Object Detection and Classification.' in Manoj Kumar Mishra, Bhabani Shankar Prasad Mishra, Yashwant Singh Patel and Rajiv Misra (eds.), *Smart Techniques for a Smarter Planet: Towards Smarter Algorithms* (Springer International Publishing: Cham).
- Weih, Robert C., and Norman D. Riggan. 2010. "Object-based classification vs. Pixel-based classification: Comparative importance of multi-resolution imagery." In.
- Woinarski, John CZ, Sally L South, Paul Drummond, Gregory R Johnston, and Alex Nankivell. 2017. 'The diet of the feral cat (*Felis catus*), red fox (*Vulpes vulpes*) and dog (*Canis familiaris*) over a three-year period at Witchelina Reserve, in arid South Australia', *Australian Mammalogy*, 40: 204-13.

- Wu, Tianjun, Jiancheng Luo, Lijing Gao, Yingwei Sun, Wen Dong, Ya'Nan Zhou, Wei Liu, Xiaodong Hu, Jiangbo Xi, Changpeng Wang, and Yun Yang. 2021. 'Geo-object-based vegetation mapping via machine learning methods with an intelligent sample collection scheme: A case study of taibai mountain, china', *Remote sensing (Basel, Switzerland)*, 13: 1-23.
- Xue, Jinru, and Baofeng Su. 2017. 'Significant Remote Sensing Vegetation Indices: A Review of Developments and Applications', *Journal of sensors*, 2017: 1-17.
- Yang, Jian, Peter J. Weisberg, and Nathan A. Bristow. 2012. 'Landsat remote sensing approaches for monitoring long-term tree cover dynamics in semi-arid woodlands: Comparison of vegetation indices and spectral mixture analysis', *Remote sensing of environment*, 119: 62-71.
- Yue, Jun, Wenzhi Zhao, Shanjun Mao, and Hui Liu. 2015. 'Spectral-spatial classification of hyperspectral images using deep convolutional neural networks', *Remote sensing letters*, 6: 468-77

9. APPENDICES

9.1 Appendix A- Map of Study Area and Witchelina Station Map

Witchelina Nature Reserve - Study Area



Removed due to copyright restriction

Department of Water, Land, and Biodiversity Conservation (2009)

9.2 Appendix B- Metadata of Pleiades Imagery

Removed due to copyright restriction

©CNES_2020, distribution AIRBUS DS, France, all rights reserved

9.3 Appendix C- Ground Control Points for UAV Survey Missions

	UTM z53 Eastings	Units:Metres Northing	Elevation (Z- value)	Area Name
1	789030.7	6669116	173.798	4d
2	789554.7	6669098	172.556	4d
3	789543.4	6668837	175.111	4d
4	789023.7	6668859	175.333	4d
5	787394.3	6667487	157.281	4e
6	787435.3	6667439	158.765	4e
7	787928.8	6668335	164.738	4f
8	788023.5	6668300	169.257	4f
9	788618.5	6668773	170.363	4g
10	788565.4	6668687	169.573	4g
11	794085.9	6673638	153.144	1e
12	794067.9	6673557	154.525	1e
13	794488.3	6672572	145.857	1f
14	794548.3	6672584	145.74	1f
15	794652.6	6671672	139.943	1a
16	794732.9	6671650	139.496	1a
17	794587.1	6671218	141.261	1d
18	794551.7	6671266	141.615	1d
19	795009	6671700	138.74	1b
20	795084.4	6671596	138.477	1b
21	794870.8	6671231	139.637	1c
22	794956.5	6671252	139.198	1c
23	794717.5	6670247	141.613	2a
24	794836.1	6670181	140.521	2a

25	794798.8	6669963	141.972	2d
26	794900.9	6669902	140.832	2d
27	795236.6	6670298	140.214	2b
29	795483.8	6670246	138.333	2b
30	795553.6	6670122	140.405	2c
31	795492.7	6670091	139.302	2c

9.3 Appendix D- Field Notes taken using Survey 123

Available at: <https://arcg.is/WynrG0>

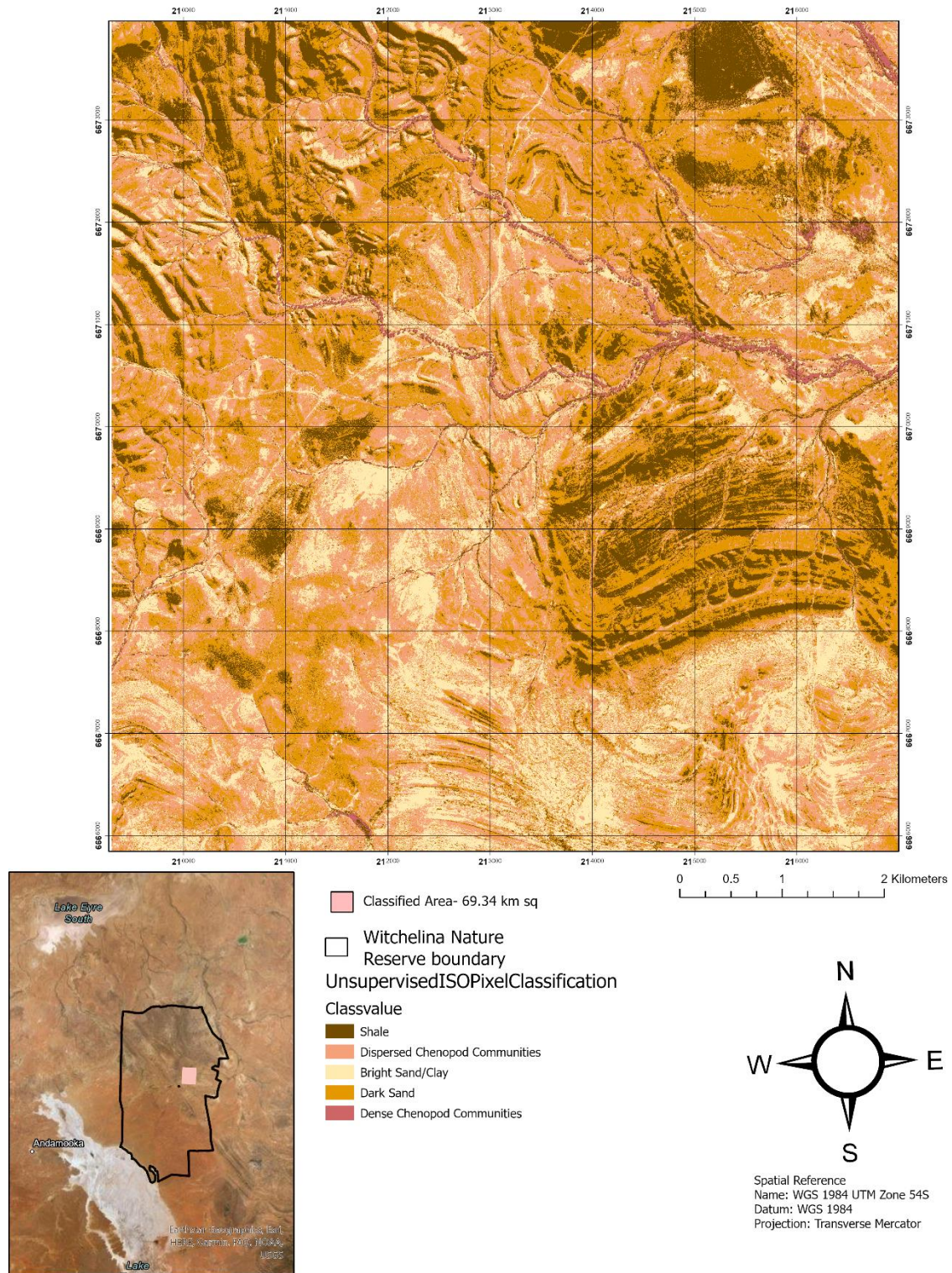
9.4 Appendix E- Maps of Classification Results

Results from Object based image segmentation using SVM and Object-based image classification Using Deep Learning can be viewed on an online map accessible through this online URL:

<https://flindersuni.maps.arcgis.com/apps/MapSeries/index.html?appid=5789bb9946474ec9b777037366af0ed3>

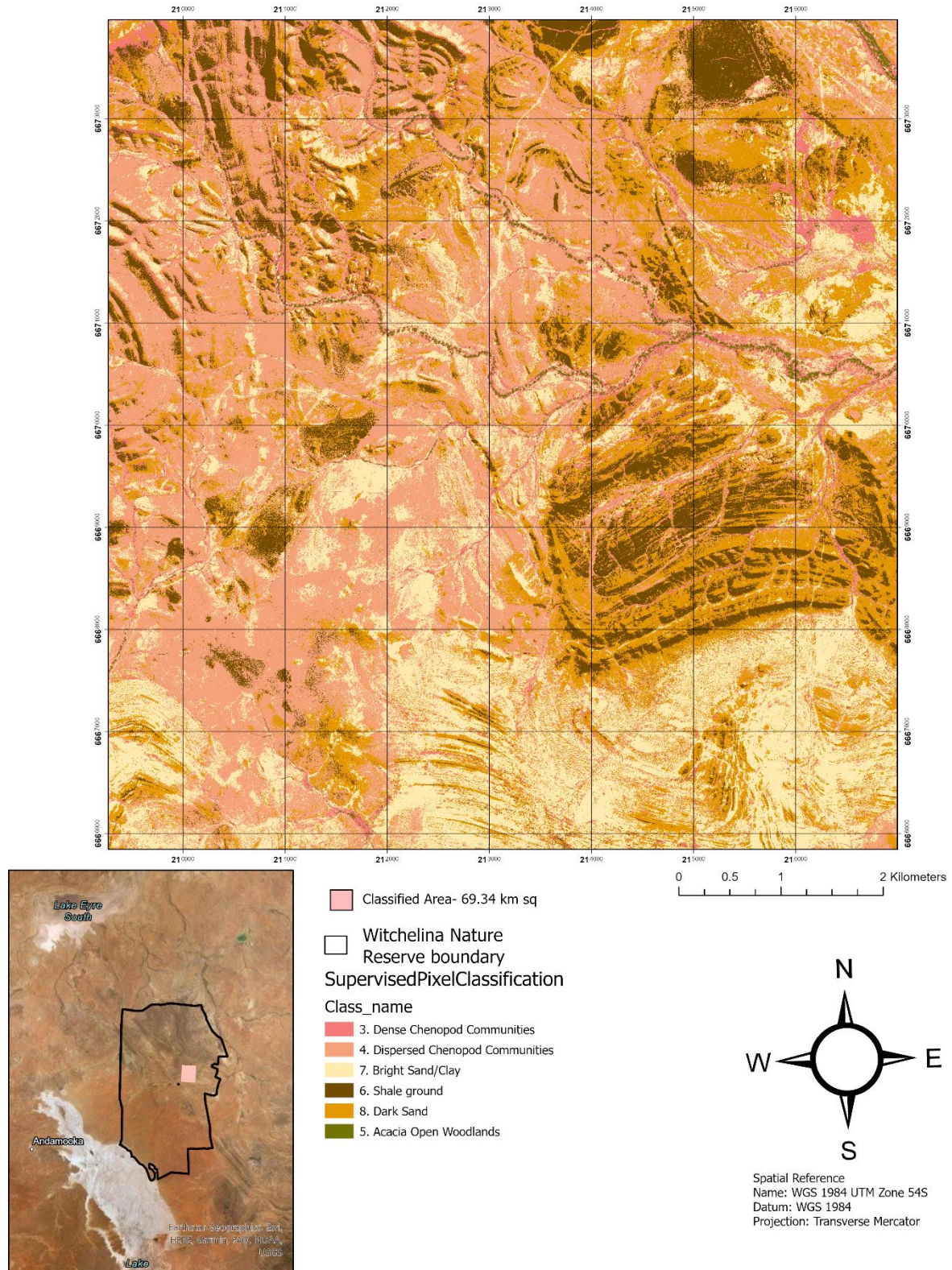
9.4.1- Unsupervised ISO Pixel Classification

Classification Output - Unsupervised ISO Pixel Classification



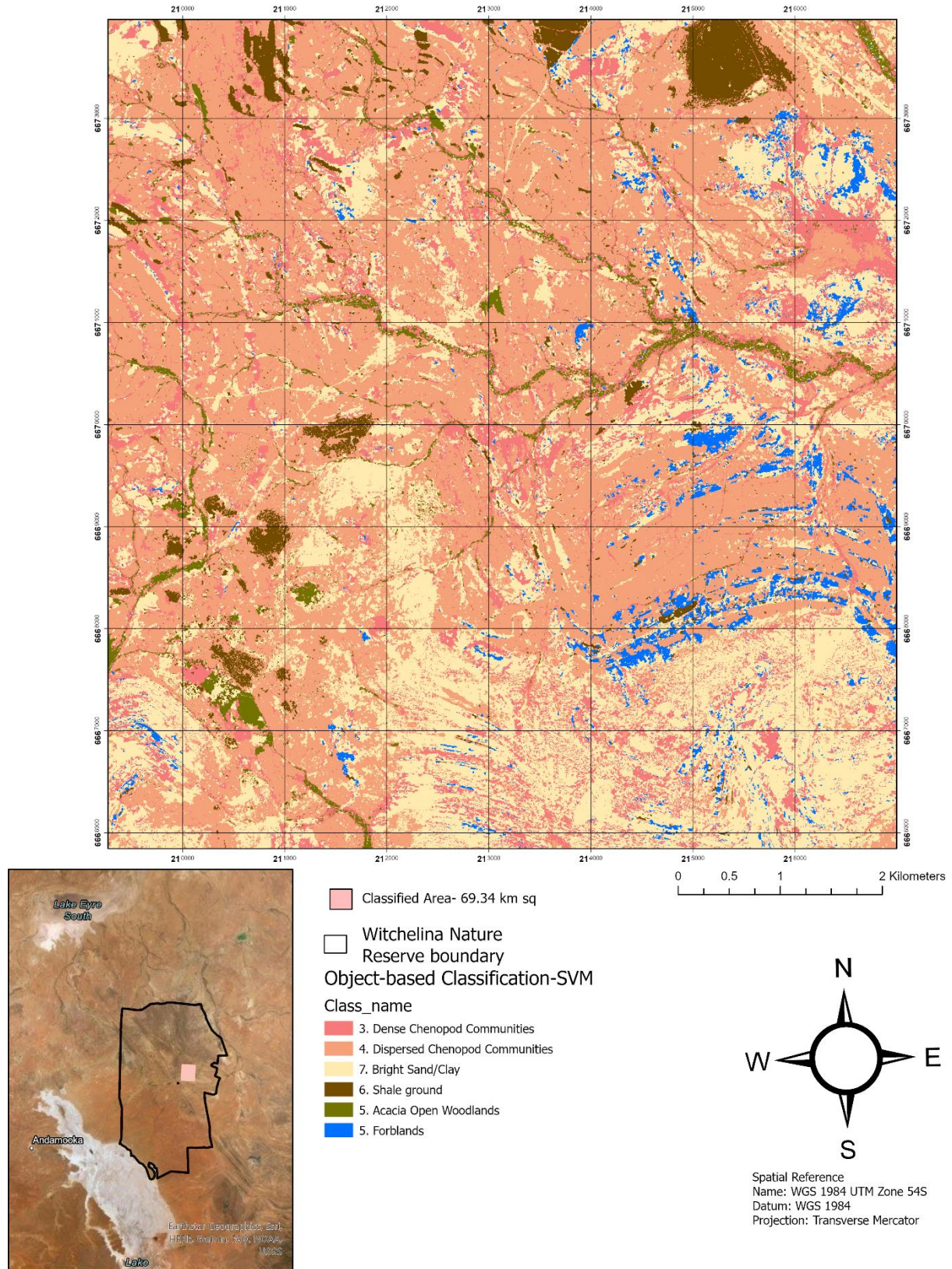
9.4.2- Supervised ML Pixel Classification

Classification Output - Supervised Pixel Classification- Maximum Likelihood



9.4.3- Object-based Image Segmentation- SVM

Classification Output - Object-based Image Classification- SVM



9.4.4- Object-based Image Classification using Deep Learning

Classification Output - Object-based Image Classification- Deep Learning 64*64

